iScience

CellPress
OPEN ACCESS

Article

Mixed lineage kinase-like protein protects against *Clostridium perfringens* infection by enhancing NLRP3 inflammasome-extracellular traps axis

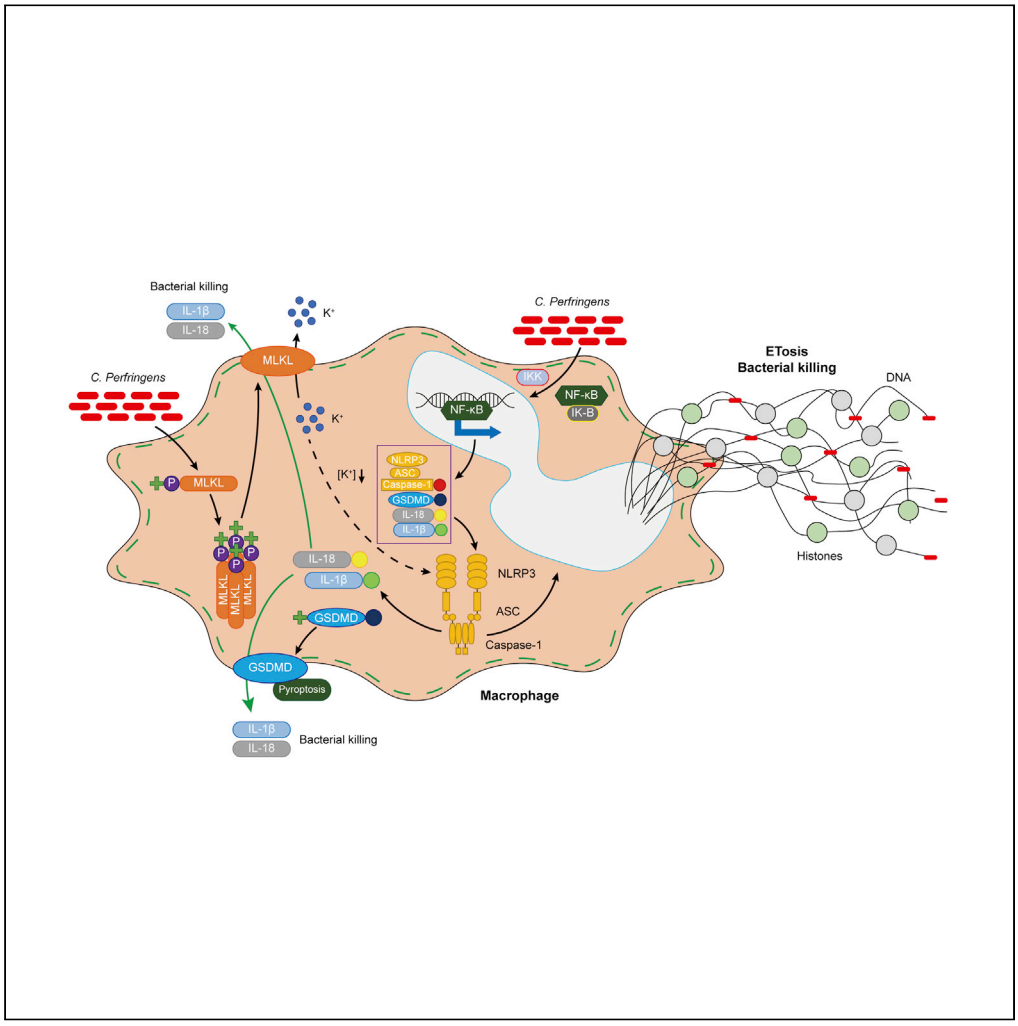

Yang Liu, Li-Hua Xing, Fen-Xin Li, ..., Guang-Peng Li, Xiao Wang, Shui-Xing Yu

wangxiao@imu.edu.cn (X.W.)
shuixingyu@imu.edu.cn (S.-X.Y.)

Highlights

MLKL is critical in limiting *Clostridium perfringens* gas gangrene and enterocolitis

MLKL deficiency leads to impaired potassium efflux-dependent NLRP3 signaling

MLKL mediates NLRP3 inflammasome signaling for extracellular traps formation

MLKL-NLRP3-extracellular traps axis facilitates pathogen control *in vitro* and in mice

Liu et al., iScience *25*, 105121
October 21, 2022
https://doi.org/10.1016/j.isci.2022.105121

iScience

CellPress
OPEN ACCESS

Article

Mixed lineage kinase-like protein protects against *Clostridium perfringens* infection by enhancing NLRP3 inflammasome-extracellular traps axis

Yang Liu,[1,3] Li-Hua Xing,[1,3] Fen-Xin Li,[1] Na Wang,[1] Yu-Ze Ma,[1] Jian-Wei Li,[1] Yu-Jing Wu,[1] Jing Liang,[1] Yu-Xin Lei,[1] Xue-Yin Wang,[1] Fan-Hua Meng,[1] Yong-Jun Yang,[2] Guang-Peng Li,[1] Xiao Wang,[1,*] and Shui-Xing Yu[1,4,*]

SUMMARY

Despite intense research in understanding *Clostridium perfringens* (*C. perfringens*) pathogenesis, the mechanisms by which it is cleared from the host are largely unclarified. In *C. perfringens* gas gangrene and enterocolitis model, *Mlkl*$^{-/-}$ mice, lacking mixed lineage kinase-like protein (MLKL), are more susceptible to *C. perfringens* infection. *Mlkl* deficiency results in a defect in inflammasome activation, and IL-18 and IL-1β releases. Exogenous administration of recombinant IL-18 is able to rescue the susceptibility of *Mlkl*$^{-/-}$ mice. Notably, K^+ efflux-dependent NLRP3 inflammasome signaling downstream of active MLKL promotes bacterial killing and clearance. Interestingly, the defect of bactericidal activity is also mediated by decreased classical extracellular trap formation in the absence of *Mlkl*. Our results demonstrate that MLKL mediates extracellular trap formation in a NLRP3 inflammasome-dependent manner. These findings highlight the requirement of MLKL for host defense against *C. perfringens* infection through enhancing NLRP3 inflammasome-extracellular traps axis.

INTRODUCTION

C. perfringens is a clinically significant opportunistic pathogen. This Gram-positive and rod-shaped bacterium is found ubiquitously in the environment, and in uncooked and processed food. *C. perfringens* can cause several diseases, including gas gangrene, food poisoning, and antibiotic-associated diarrhea. Today, traumatic injury is responsible for up to 70% of the cases of clostridial gas gangrene (Ahrenholz, 1988), and radical amputation is still a favorable treatment of choice for severe *C. perfringens* gas gangrene. The Centers for Disease Control and Prevention (CDC) estimates that *C. perfringens* causes nearly 1 million foodborne illnesses in the United States every year (Grass et al., 2013). Generally, individuals experience abdominal pain, stomach cramps, and diarrhea within 6-24 h after consuming *C. perfringens*-contaminated food. At present, the treatment recommendation is a combination of a broad-spectrum synergistic penicillin combination with clindamycin or a carbapenem, despite growing scientific concern over antibiotic resistance (Lee et al., 2019). Although there has been a great deal of research in understanding pathogenesis, the precise mechanisms by which *C. perfringens* is cleared from the host remain to be unveiled, thus delaying the development of novel strategies for control of this infection.

The host innate immune system provides the first line of recognition and elimination of invading pathogens. The innate immune response to pathogen infection is initiated by the recognition of microbial-derived moieties, termed pathogen-associated molecular patterns (PAMPs), such as exotoxins, nucleic acids, lipopolysaccharide, teichoic-acid, peptidoglycan, and flagellin (Zhivaki and Kagan, 2021; Rathinam et al., 2019). Indeed, PAMPs are recognized by several families of innate receptors, including the NOD-like receptors (Tourlomousis et al., 2020), the Toll-like receptors (Mathur et al., 2012), the C-type lectin receptors (Roesner et al., 2019), the RIG-like helicases (Asaka et al., 2009), and cytosolic DNA sensors (Sisquella et al., 2017), which in turn help to detect invading pathogenic microbes and prevent disease progression. Growing evidence indicates that *C. perfringens* interact with the host to drive the innate response, and Toll-like receptors and NOD-like receptors were implicated in *C. perfringens* recognition (Huang et al., 2019; Yamamura et al., 2019). Hence, investigating the innate immune mechanisms of host resistance to *C. perfringens* will be conducive to implementing pathogen control strategies.

[1]State Key Laboratory of Reproductive Regulation and Breeding of Grassland Livestock, College of Life Sciences, Inner Mongolia University, Hohhot 010070, China

[2]Key Laboratory of Zoonosis Research, Ministry of Education, College of Veterinary Medicine, Jilin University, Changchun 130062, China

[3]These authors contributed equally

[4]Lead contact

*Correspondence: wangxiao@imu.edu.cn (X.W.), shuixingyu@imu.edu.cn (S.-X.Y.)

https://doi.org/10.1016/j.isci.2022.105121

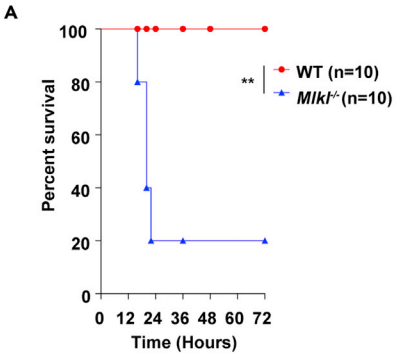
A
100
80
60
40
20
0
Percent survival
0 12 24 36 48 60 72
Time (Hours)
**
WT (n=10)
Mlkl-/- (n=10)

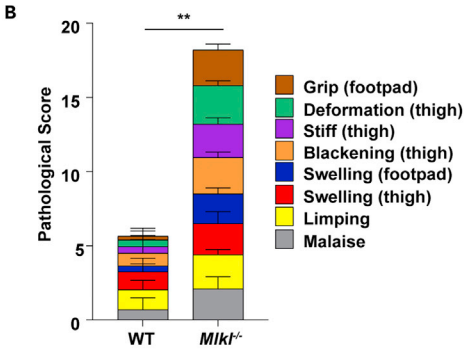
B
20
15
10
5
0
Pathological Score
**
WT
Mlkl-/-
Grip (footpad)
Deformation (thigh)
Stiff (thigh)
Blackening (thigh)
Swelling (footpad)
Swelling (thigh)
Limping
Malaise

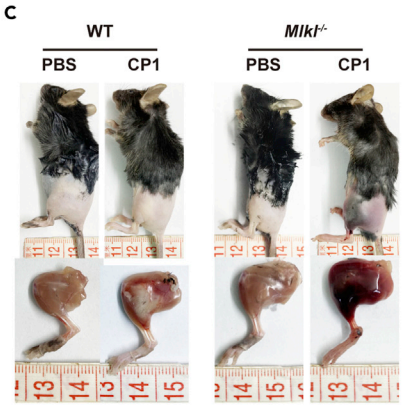
C
WT
Mlkl-/-
PBS
CP1
PBS
CP1

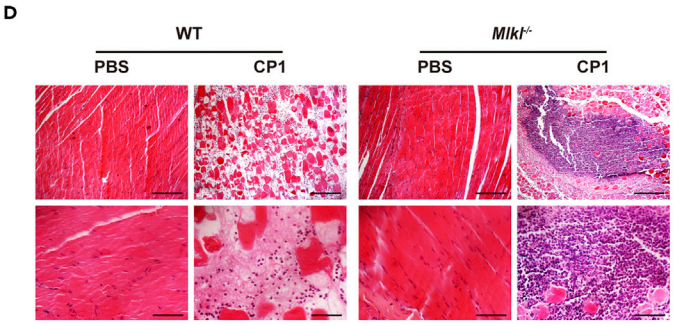
D
WT
Mlkl-/-
PBS
CP1
PBS
CP1

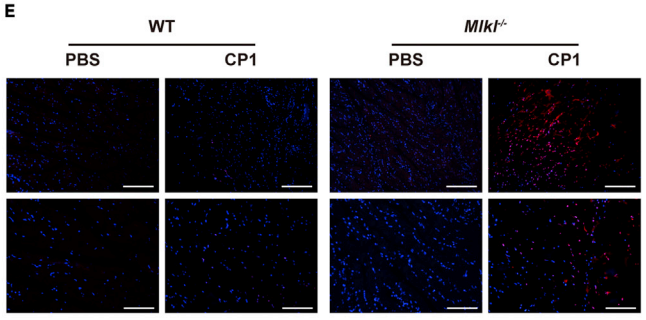
E
WT
Mlkl-/-
PBS
CP1
PBS
CP1

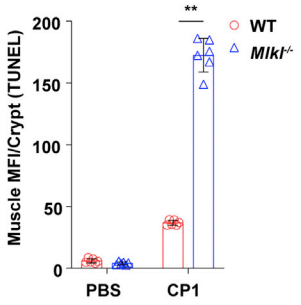
**
WT
Mlkl-/-
Muscle MFI/Crypt (TUNEL)
200
150
100
50
0
PBS
CP1

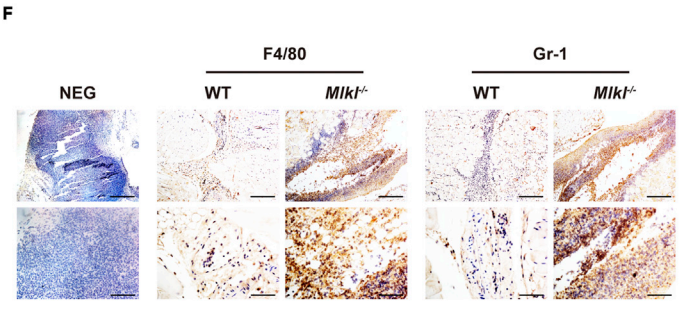
F
NEG
F4/80
Gr-1
WT
Mlkl-/-
WT
Mlkl-/-

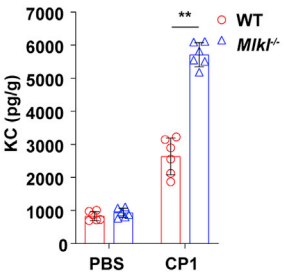
G
**
WT
Mlkl-/-
KC (pg/g)
7000
6000
5000
4000
3000
2000
1000
0
PBS
CP1

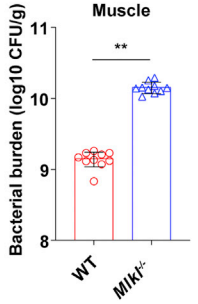
H
Muscle
**
Bacterial burden (log10 CFU/g)
11
10
9
8
WT
Mlkl-/-

Figure 1. MLKL is sufficient to protect against *C. perfringens* gas gangrene

Six to eight-weeks-old sex-matched WT and *Mlkl*$^{-/-}$ mice were intramuscularly infected with *C. perfringens*.

(A) Survival (5 × 10^7 CFU, n = 10 each group).

(B) Cumulative gross pathology scores of infected mice (5 × 10^7 CFU, n = 10 each group).

(C) Representative pathologic photographs of the leg tissue of mice (1 × 10^7 CFU, n = 10 each group, at 24 h p.i.).

(D) Representative H&E staining of muscle tissue (1 × 10^7 CFU, n = 10 each group, at 24 h p.i., upper panel, magnification ×100, lower panel, magnification, ×400).

(E) Representative TUNEL staining of apoptotic cells in the muscle tissue (upper panel, magnification ×100, lower panel, magnification, ×200).

(F) Representative immunohistochemical staining of F4/80 (a macrophagocyte marker) and Gr-1 (a neutrophil marker) was performed in the muscle sections (upper panel, magnification ×100, lower panel, magnification, ×400).

(G) The homogenate supernatant of muscle was detected for the concentration of indicated chemokine KC by ELISA.

(H) Bacterial load in the muscle was detected (1 × 10^7 CFU, n = 10 each group, at 24 h p.i.).

NEG, primary antibody omitted. Graphs are means ± SD from data pooled from ten (B and H) or six (E and G) biological replicates. Data were considered significant when $^{**}p < 0.01$.

The mixed lineage kinase-like protein (MLKL), is an essential necroptosis effector that operates downstream of the receptor-interacting protein kinase 1 and 3 necrosome complex (Petrie et al., 2018). The MLKL phosphorylation event is thought to trigger a molecular switch leading to the exposure of the N-terminal four-helix bundle structural domain, its oligomerization, membrane translocation, and eventually cell death (Tanzer et al., 2016). As its function as a necroptosis effector was disclosed, research on MLKL has mainly focused on its role in innate immunity when the necroptosis process is initiated. Recently, several studies including ours have demonstrated that MLKL-mediated necroptosis is predominant in serious inflammatory diseases and implicated in pathogens infection (McComb et al., 2014; Yu et al., 2017). Particularly, we have previously reported that non-hematopoietic MLKL contributes to the maintenance of intestinal integrity in a necroptosis-independent manner and protects against *Salmonella* mucosal infection (Yu et al., 2018). Obviously, necroptosis modulator does not seem to be the sole responsibility of active MLKL.

Here, we sought to characterize the biological implications of MLKL in response to *C. perfringens* infection, including the possibility that it might elicit innate host immunity. Indeed, we find that MLKL protects the host against *C. perfringens* gas gangrene and enterocolitis. *Mlkl*$^{-/-}$ mice exhibit higher mortality rates, more bacterial burden, and severer organ damage compared to control mice. Mechanistically, *Mlkl* deficiency leads to impaired K^+ efflux-dependent NLRP3 inflammasome signaling and extracellular traps formation, which facilitates bacterial growth and proliferation. Interestingly, MLKL-mediated extracellular traps release in response to *C. perfringens* is dependent on NLRP3 inflammasome activation. Collectively, our results reveal that MLKL is essential for host defense against *C. perfringens* infection through enhancing NLRP3 inflammasome-extracellular traps axis to promote bactericidal activity.

RESULTS

Mixed lineage kinase-like protein contributes to host protection against *C. perfringens* gas gangrene

Using *C. perfringens* gas gangrene model, we initially explored the possible involvement of MLKL in the host response to *C. perfringens* infection. WT and *Mlkl*$^{-/-}$ mice were intramuscularly infected with 5 × 10^7 CFU of representative *C. perfringens* strain CP1 (a clinical isolate of *C. perfringens*, specific 16S rDNA gene sequence data deposited at NCBI GenBank : MW440585), and the mortality of mice were monitored over 72 h. At 22 h p.i., we observed that almost 80% of *Mlkl*$^{-/-}$ mice had died, whereas all of the WT mice remained alive (Figure 1A). Meanwhile, *Mlkl*$^{-/-}$ mice exhibited more severe clinical symptoms, demonstrated by grip loss, intense stiff, blackening, deformation, swelling, malaise, and limping (Figure 1B). The experiment was repeated with a lower infective dose of *C. perfringens* strain CP1 (1 × 10^7 CFU per mouse) to study the phenotype of *Mlkl*$^{-/-}$ mice under milder conditions. In accordance with the high level of mortality, the legs of *C. perfringens*-infected *Mlkl*$^{-/-}$ mice also tended to be markedly red and swollen, accompanied by extensive hyperemia and hemorrhagic clots (Figure 1C). These clinical assessments were validated by the histologic analysis of muscle. *Mlkl*$^{-/-}$ mice had more severe histological damage and exacerbated tissue inflammation compared with WT mice, demonstrated by destroyed muscle architecture, elevated cell death, massive PMN infiltration, and increased expression of chemokine KC (Figures 1D–1G). To further determine whether the decreased survival and severe pathology in *Mlkl*$^{-/-}$ mice during *C. perfringens* infection might link to higher bacterial burdens, bacterial numbers in muscle were enumerated at 24 h p.i. As expected, significantly more bacteria were detected in the muscles of

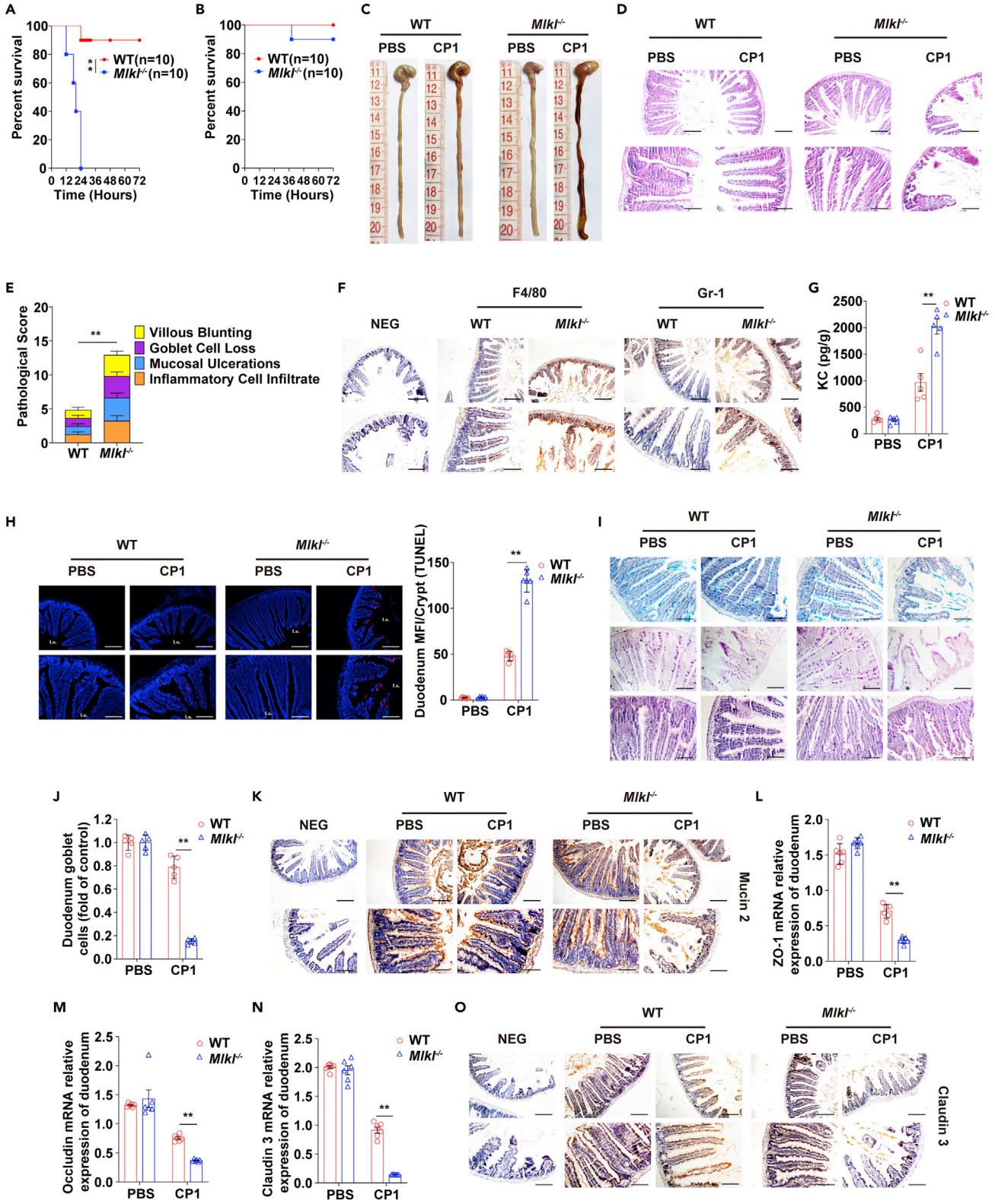

Figure 2. *Mlkl* deficiency leads to increased duodenal injury during *C. perfringens* mucosal infection

D-4-Amino-3-isoxazolidinone-pretreated WT and *Mlkl*$^{-/-}$ mice were orally infected with *C. perfringens*.

(A) Survival (2 × 10^8 CFU, n = 10 each group).

Figure 2. *Continued*

(B) Survival (1 × 10^8 CFU, n = 10 each group).

(C) Representative gross appearance of duodenum (1 × 10^8 CFU, n = 10 each group, at 24 h p.i.).

(D and E) Representative H&E staining of duodenal tissue and pathological scores (1 × 10^8 CFU, n = 10 each group, at 24 h p.i., upper panel, magnification ×100, lower panel, magnification, ×200).

(F) Representative F4/80 and Gr-1 (IHC) stained brown (upper panel, magnification ×100, lower panel, magnification, ×200).

(G) The homogenate supernatant of duodenum was examined for the concentration of indicated chemokine KC by ELISA.

(H) Representative TUNEL staining of apoptotic cells in the duodenal tissue (upper panel, magnification ×100, lower panel, magnification, ×200).

(I and J) Total mucins expression in goblet cells was examined via PAS staining (magnification, ×200).

(K) Representative mucin 2 (IHC) stained brown (upper panel, magnification ×100, lower panel, magnification, ×200).

(L–N) The mRNA levels of ZO-1, Occludin, and Claudin 3 in duodenum were determined by qRT-PCR. The data were normalized to GAPDH expression and are shown as the fold increase in mRNA.

(O) Representative claudin 3 (IHC) stained brown (upper panel, magnification ×100, lower panel, magnification, ×200).

NEG, primary antibody omitted. Graphs are means ± SD from data pooled from ten (E) or five to six (G, H, J, L, M and N) biological replicates. Data were considered significant when $^{**}p < 0.01$.

Mlkl$^{-/-}$ mice compared with WT mice (Figure 1H). Thus, these data suggest that MLKL plays an indispensable role in protection against *C. perfringens* gas gangrene.

Mixed lineage kinase-like protein is critical in limiting *C. perfringens* enterocolitis

Next, we asked if MLKL also regulated host defense against *C. perfringens* mucosal infection, as *C. perfringens* is one of the most prevalent foodborne pathogens. WT and *Mlkl*$^{-/-}$ mice were orally infected with 2 × 10^8 CFU of representative *C. perfringens* strain CP1, and animal mortality was then monitored for 72 h. Compared to WT counterparts, *Mlkl*$^{-/-}$ mice demonstrated a significantly lower survival rate. At 24 h p.i., we observed that all of *Mlkl*$^{-/-}$ mice had died, whereas almost 90% of WT mice remained alive (Figure 2A). The experiment was repeated with a sublethal dose of *C. perfringens* strain CP1 (1 × 10^8 CFU per mouse) to study the phenotype of *Mlkl*$^{-/-}$ mice under milder conditions (Figure 2B). In accordance with the high level of mortality, duodenal injury was more severe in *Mlkl*$^{-/-}$ mice compared with WT mice, demonstrated by extensive hyperemia and hemorrhage, complete destruction of epithelial integrity, large mucosal ulcerations, severe villous blunting, goblet cell loss, massive PMN infiltration, and elevated expression of chemokine KC (Figures 2C–2G). Epithelial barrier integrity, as measured by tissue homeostasis, and the expression of mucoproteins and tight junction proteins, was obviously disrupted in *Mlkl*$^{-/-}$ mice. *Mlkl* deficiency results in greatly increased numbers of TUNEL-positive epithelial cells (Figure 2H), dramatically reduced the expression of AB-PAS staining mucins and mucin 2 (Figures 2I–2K), and significantly decreased the expression of tight junction including zonula occludens (ZO)-1, occludin and claudin 3 (Figures 2L–2O) than in those of WT mice, indicating that MLKL alleviates the disruption of mucosal barrier integrity following *C. perfringens* infection.

To gain additional evidence of the role of MLKL in host defense against mucosal *C. perfringens* infection, the pathologic changes in cecum were further determined. In accordance with the severe duodenal damage, *Mlkl*$^{-/-}$ mice also tended to lose more cecal weight compared to WT mice (Figure 3A). Meanwhile, this clinical assessment was validated by the histologic analysis of cecum. *Mlkl*$^{-/-}$ mice had severe cecal damage and exacerbated cecal inflammation, demonstrated by complete destruction of epithelial integrity, intense submucosal edema, goblet cell loss, massive inflammatory cells infiltration, and increased expression of chemokine KC (Figures 3B–3E). Similarly, the exaggerated loss of the mucosal barrier integrity in *Mlkl*$^{-/-}$ mice during *C. perfringens* infection, revealed by increased numbers of TUNEL-positive epithelial cells (Figure 3F), reduced the expression of AB-PAS staining mucins and mucin 2 (Figures 3G–3I), and decreased the expression of tight junction such as ZO-1, occludin, and claudin 3 (Figures 3J–3M). Subsequently, to further determine whether a defect in bacterial clearance contributes to the susceptible of *Mlkl*$^{-/-}$ mice during *C. perfringens* mucosal infection, the bacterial load at the mucosal site and systemic site were assessed at 24 h p.i. As compared with WT mice, *Mlkl*$^{-/-}$ mice harbored markedly elevated loads of bacteria in the duodenum, cecum, MLN, liver, and spleen (Figure 3N). Conclusively, these results suggested that MLKL is essential for the host defense against *C. perfringens*-induced enterocolitis.

Mixed lineage kinase-like protein -mediated inflammasome activation restricts bacterial colonization

As previous research has shown that inflammasome activation emerges as an important aspect of host defense against invading pathogens (Chudnovskiy et al., 2016; Yu et al., 2018). To confirm whether there is a

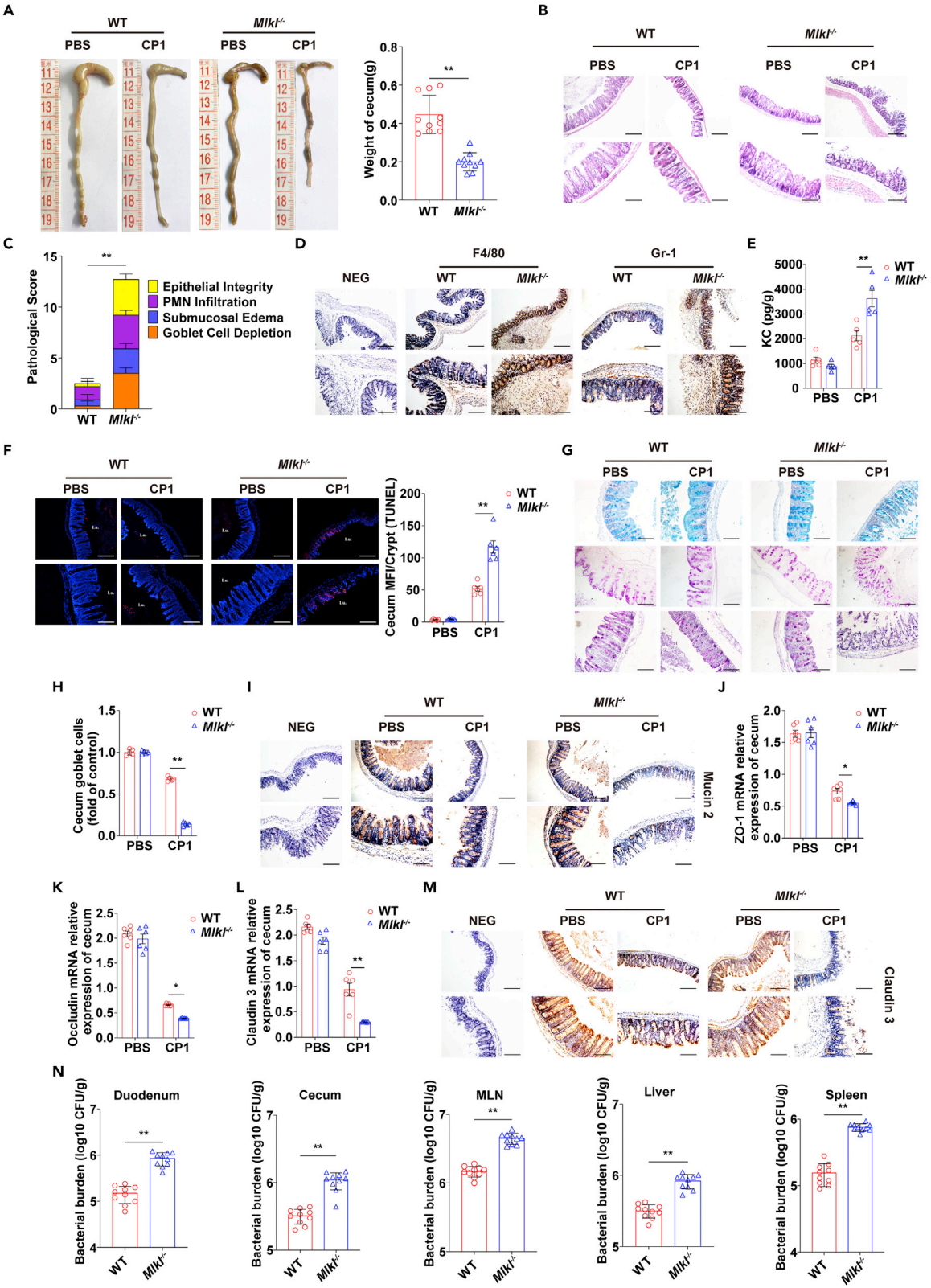
A
WT
Mlkl-/-
PBS
CP1
Weight of cecum(g)
B
C
Pathological Score
Epithelial Integrity
PMN Infiltration
Submucosal Edema
Goblet Cell Depletion
D
NEG
F4/80
Gr-1
E
KC (pg/g)
F
Cecum MFI/Crypt (TUNEL)
G
H
Cecum goblet cells (fold of control)
I
Mucin 2
J
ZO-1 mRNA relative expression of cecum
K
Occludin mRNA relative expression of cecum
L
Claudin 3 mRNA relative expression of cecum
M
Claudin 3
N
Duodenum
Cecum
MLN
Liver
Spleen
Bacterial burden (log10 CFU/g)

Figure 3. *Mlkl* deficiency results in severe cecal damage following *C. perfringens* mucosal infection

D-4-Amino-3-isoxazolidinone-pretreated WT and *Mlkl*$^{-/-}$ mice were orally infected with *C. perfringens*.

(A) Representative pathologic photographs and weight of the cecum (1 × 10^8 CFU, n = 10 each group, at 24 h p.i.).

(B and C) Representative H&E staining of the cecum tissue and pathological scores (1 × 10^8 CFU, n = 10 each group, at 24 h p.i., upper panel, magnification ×100, lower panel, magnification, ×200).

(D) Representative F4/80 and Gr-1 (IHC) stained brown (upper panel, magnification ×100, lower panel, magnification, ×200).

(E) The homogenate supernatant of cecum was examined for the concentration of indicated chemokine KC by ELISA.

(F) Representative TUNEL staining of apoptotic cells in the cecal tissue (upper panel, magnification ×100, lower panel, magnification, ×200).

(G and H) Total mucins expression in goblet cells was examined via PAS staining (magnification, ×200).

(I) Representative mucin 2 (IHC) stained brown (upper panel, magnification ×100, lower panel, magnification, ×200).

(J–L) The cecum tissue mRNA was examined for ZO-1, Occludin, and Claudin 3 by qRT-PCR. The data were normalized to GAPDH expression and are shown as the fold increase in mRNA.

(M) Representative claudin 3 (IHC) stained brown (upper panel, magnification ×100, lower panel, magnification, ×200).

(N) Bacterial burden in the duodenum, cecum, MLN, liver, and spleen were quantitated (1 × 10^8 CFU, n = 10 each group, at 24 h p.i.).

NEG, primary antibody omitted. Graphs are means ± SD from data pooled from ten (A and C) or five to six (E, F, H, J, K, and L) biological replicates. Data were considered significant when *p < 0.05 or **p < 0.01.

difference in inflammasome activation that can explain the increased susceptibility of *Mlkl*$^{-/-}$ mice to *C. perfringens* infection, we first evaluated inflammasome signaling. Strikingly, the inflammasome-dependent Caspase-1 cleavage dramatically reduced in the muscle, duodenum, and cecum tissues of infected *Mlkl*$^{-/-}$ mice relative to the levels observed in those of infected WT mice, although the expression of ASC did not appear significantly different (Figures 4A–4C). Importantly, the production of mature IL-1β and IL-18 was also significantly inhibited in the muscle, duodenum, and cecum tissues of infected *Mlkl*$^{-/-}$ mice compared with infected WT controls (Figures 4A–4F). However, TNF-α expression was comparable between both genotypes (Figures 4G–4I). Thus, *Mlkl* deficiency potently results in attenuated inflammasome activation following *C. perfringens* infection. We next asked if MLKL-mediated inflammasome activation was involved in protection against *C. perfringens* infection, *Mlkl*$^{-/-}$ mice were treated prophylactically (day-1 and day 0 of infection) with rIL-18 and determined whether exogenous administration of IL-18 could rescue the susceptibility to infection in the absence of *Mlkl*. Infected *Mlkl*$^{-/-}$ mice treated with rIL-18 showed obviously alleviated pathological damage in muscle, duodenum, and cecum tissues (Figures 4J–4L). Indeed, rIL-18 administration also strongly reduced the bacterial burden in *Mlkl*$^{-/-}$ mice, measured by the levels of viable bacteria in muscle, duodenum, cecum, MLN, liver, and spleen (Figures 4M–4R). Collectively, these results showed that inflammasome activation is critical for MLKL-facilitated pathogen control.

NLRP3 inflammasome is required for mixed lineage kinase-like protein-mediated host defense

To further characterize the role of MLKL in host defense against *C. perfringens* infection, the expression of phosphorylated MLKL (*p*-MLKL) in the sections of muscle, duodenum, and cecum was investigated by immunohistochemical staining. Our results indicated that *p*-MLKL staining was predominantly located in the recruited inflammatory cells of the infected tissues (Figures 5A–5C). Subsequently, to determine whether NLRP3 inflammasome activation is involved in MLKL-mediated host defense, LPS-primed BMDMs derived from WT mice and *Nlrp3*$^{-/-}$ mice were stimulated with *C. perfringens* strain ATCC13124, CP1, CP3 or ATP (a conventional NLRP3 inflammasome agonist), respectively. As shown in Figures 5D–5G, 5P, and 5Q, inflammasome signaling was markedly inhibited in *Nlrp3*$^{-/-}$ macrophages vs. WT macrophages, indicated by impaired Caspase-1 and IL-1β cleavages, decreased mature IL-1β and IL-18 release, and reduced LDH activity and ASC speck formation, whereas LPS-dependent TNF-α secretion was not inhibited in the absence of *Nlrp3*, indicating that *C. perfringens* surely induced NLRP3 inflammasome activation. Recently, K^+ efflux is widely proposed as a specific upstream requirement for NLRP3 inflammasome activation and increasing the extracellular [K^+] inhibits NLRP3 inflammasome activation (Munoz-Planillo et al., 2013), although there is evidence that some NLRP3 activators induce NLRP3 inflammasome activation in a K^+ efflux-independent mechanism (Groß et al., 2016). To understand the mechanism whereby *C. perfringens* induces NLRP3 inflammasome, we sought to investigate whether K^+ efflux is required for *C. perfringens*-induced NLRP3 inflammasome activation. Extracellular potassium of 50 mM provides obvious inhibition of NLRP3 inflammasome activation by *C. perfringens* challenged, revealed by impaired Caspase-1, GSDMD, and IL-1β cleavages, and reduced mature IL-1β and IL-18 release, and decreased LDH activity, although LPS-dependent TNF-α secretion was not suppressed by high concentrations of extracellular potassium (Figures 5H–5K). Thus, these findings suggested that *C. perfringens* induces NLRP3 inflammasome activation in a K^+ efflux-dependent process. We next asked

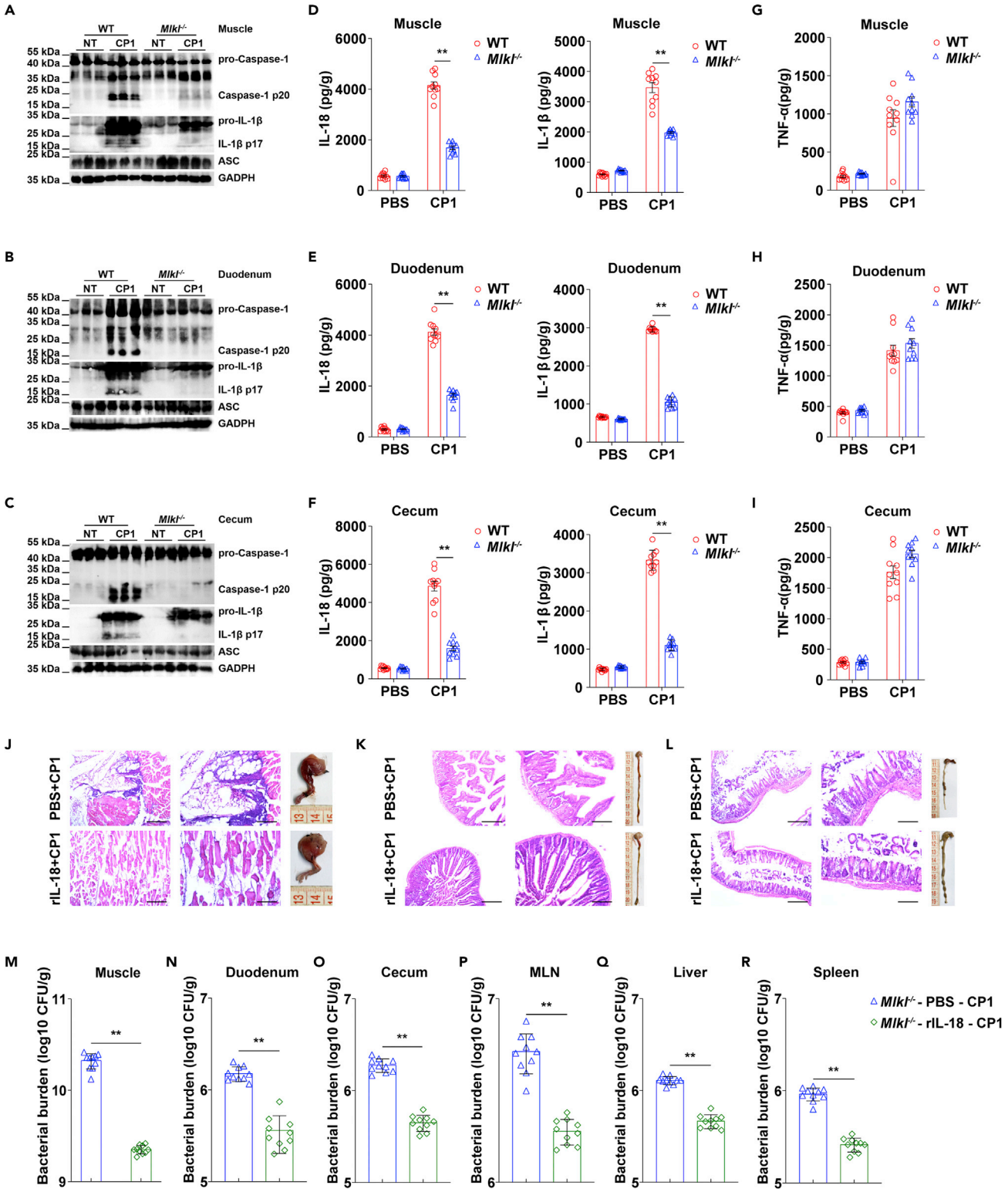

Figure 4. Inflammasome signaling downstream of MLKL confers host resistance to *C. perfringens* infection

WT and *Mlkl*$^{-/-}$ mice were intramuscularly infected with *C. perfringens* (1 × 10^7 CFU, n = 10 each group) for 24 h

(A) The muscle tissue lysate was analyzed for Caspase-1, IL-1β, and ASC by Western blotting. GAPDH was used as a loading control.

(D and G) The homogenate supernatant of the muscle tissue was analyzed for the presence of IL-18, IL-1β, and TNF-α protein using ELISA.

Figure 4. *Continued*

(M) Bacterial load in the muscle was detected. D-4-Amino-3-isoxazolidinone-pretreated WT and *Mlkl*$^{-/-}$ mice were orally infected with *C. perfringens* (1 × 10^8 CFU, n = 10 each group) for 24 h

(B and C) Duodenal and cecal tissues were collected and homogenized, and then immunoblotting for Caspase-1, IL-1β, ASC, and GAPDH, respectively.

(E, F, H, and I) Levels of IL-18, IL-1β, and TNF-α in duodenum or cecum were determined by ELISA. For one group of *Mlkl*$^{-/-}$ mice, 1.0 μg recombinant IL-18 was injected intraperitoneally daily starting the day prior to the intramuscularly or orally challenged with *C. perfringens* (n = 10 each group, at 24 h p.i.).

(J) Representative H&E staining and pathologic photographs of the muscle tissue (1 × 10^7 CFU, left panel, magnification ×100, right panel, magnification, ×400).

(K and L) Representative H&E staining and pathologic photographs of the duodenum and cecum tissues (1 × 10^8 CFU, left panel, magnification ×100, right panel, magnification, ×200).

Bacterial burdens in the duodenum (N), cecum (O), MLN (P), liver (Q), and spleen (R) were examined. Data were considered significant when **p < 0.01.

if *Mlkl* deficiency impaired K^+ efflux-dependent NLRP3 inflammasome signaling after *C. perfringens* challenge. Notably, K^+ efflux-dependent NLRP3 inflammasome signaling was largely inhibited in the absence of *Mlkl* during *C. perfringens* infection, showed by impaired Caspase-1, GSDMD, and IL-1β cleavages, reduced ASC speck formation, and decreased mature IL-1β and IL-18 release, and reduced LDH activity in the treated *Mlkl*$^{-/-}$ macrophages, whereas TNF-α secretion was not affected (Figures 5L–5Q). Interestingly, *Mlkl* deficiency also impaired bacterial α-toxin, heat-killed bacteria, and bacterial culture supernatants-triggered inflammasome signaling (Figures 5R–5T). Importantly, exogenous IL-18 treatment could rescue the defect of bacterial killing in *Mlkl*$^{-/-}$, *Nlrp3*$^{-/-}$, and *Caspase-1/11*$^{-/-}$ macrophages, respectively (Figures 5U–5W), indicating that *Mlkl* deficiency leads to a defect in bacterial killing by impairing NLRP3 inflammasome activation in macrophages.

Subsequently, to further illustrate the signaling mechanism that NLRP3 inflammasome activation mediates THE protective effect of MLKL, we then utilized *Nlrp3*$^{-/-}$ mice to evaluate the effect of NLRP3 on *C. perfringens* gas gangrene and enterocolitis. At 24 h p.i., similar to *Mlkl*$^{-/-}$ mice, *Nlrp3*$^{-/-}$ mice showed increased bacterial loads in muscle, duodenum, cecum, MLN, liver, and spleen (Figures 6A and 6B), indicating that there was a serious defect in the bacterial clearance of *Nlrp3*$^{-/-}$ mice as compared with WT mice. In line with this, *Nlrp3*$^{-/-}$ mice also demonstrated significantly decreased survival (Figures 6C and 6D), obvious clinical symptoms (Figures 6E–6H), and severe histological injury (Figures 6I–6K), suggesting that NLRP3 is beneficial to the host followed *C. perfringens* infection. Altogether, our data demonstrated that the protective effect of MLKL against *C. perfringens* infection is dependent on the capacity of MLKL to enhance NLRP3 inflammasome-mediated bacteria killing.

Mlkl deficiency results in the defect of extracellular traps formation

Because *Mlkl* deficiency attenuates bacterial clearance following *C. perfringens* infection, an extracellular bacterial pathogen, we delve further into the other potential mechanisms underlying MLKL in enhancing bacteria killing such as the process mediated by extracellular traps. Evidence has shown that extracellular traps release provides an extracellular site for microbial killing in the innate immune defense (Brinkmann et al., 2004; Chen et al., 2019). Factually, we find that the defect of bactericidal activity is mediated by decreased extracellular trap formation in macrophages and neutrophils in the presence of DNase I (Figures S1A and S1B). To evaluate the effect of *Mlkl* deficiency on extracellular traps formation, *C. perfringens*-challenged macrophages were contained with SYTOX Orange (a non-permeable dye that stains nucleic acid) and histone or MPO, pivotal components of extracellular traps. As expected, extracellular traps release was dramatically decreased in *Mlkl*$^{-/-}$ macrophages vs. WT macrophages (Figures 7A and 7B). To quantify extracellular traps formation, extracellular DNA content was determined in the supernatants. A reduction of extracellular DNA was seen in *Mlkl*$^{-/-}$ macrophages compared with WT macrophages (Figure 7C). Moreover, as an initial description of extracellular traps formation appeared in neutrophils (Brinkmann et al., 2004), another type of phagocyte that plays critical role in host's defense against infection, we further determined if there is a defect of extracellular trap formation in *Mlkl*$^{-/-}$ neutrophils. A similar defect of extracellular traps formation was observed in bacteria-infected *Mlkl*$^{-/-}$ neutrophils vs. WT neutrophils (Figures S2A–S2C). Correspondingly, *Mlkl* deficiency inhibits the bacterial killing capacity of neutrophil (Figure S2D). Similarly, the expression level of histone was significantly reduced in the muscle, duodenum, and cecum tissues of infected *Mlkl*$^{-/-}$ mice than in those of infected WT mice (Figures 7D and 7E). Thus, these observations suggested that *Mlkl* deficiency also resulted in the defect of extracellular traps-mediated bacteria killing.

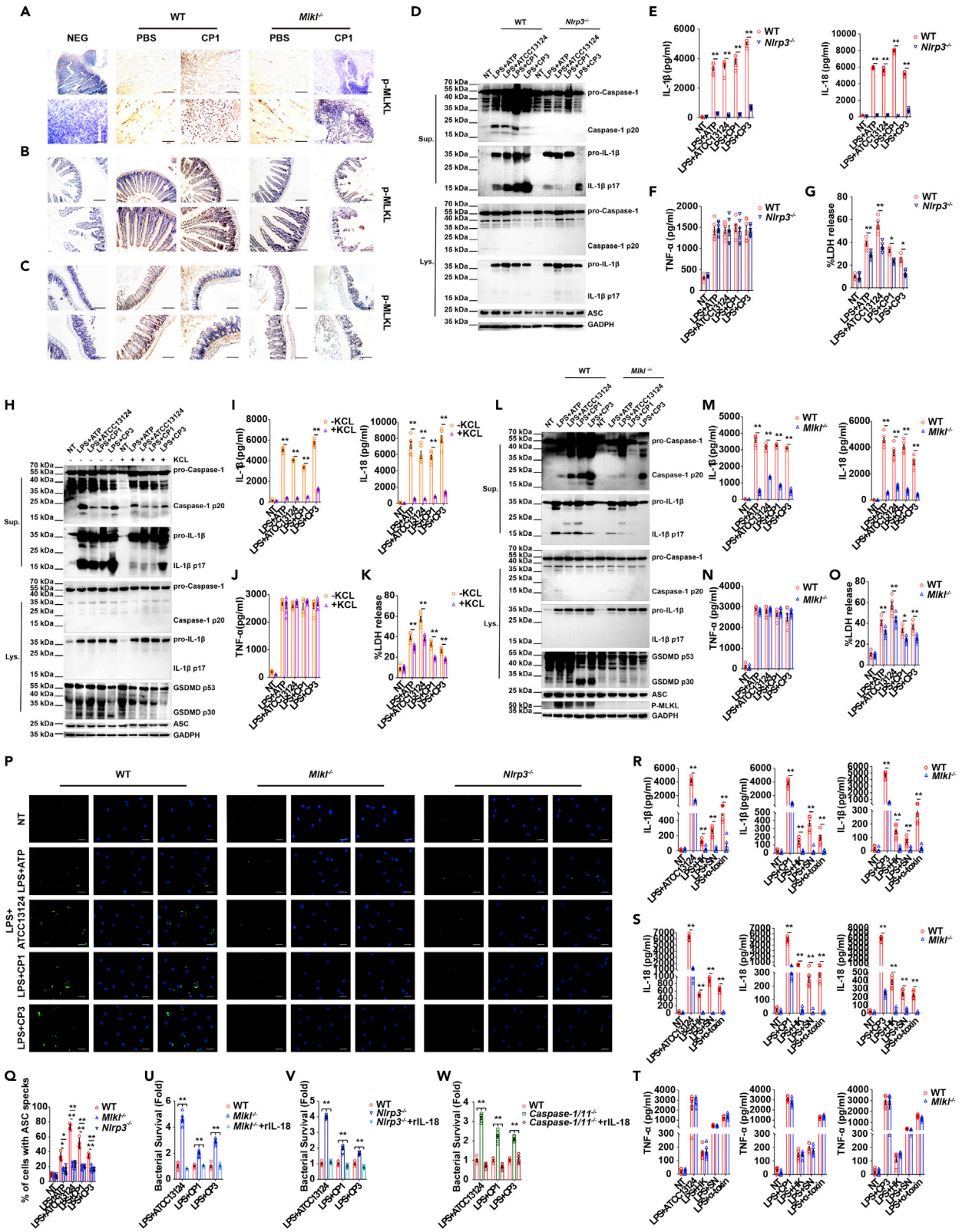
A
WT
Mlkl-/-
NEG
PBS
CP1
PBS
CP1
P-MLKL
B
P-MLKL
C
P-MLKL
D
WT
Nlrp3-/-
NT
LPS+ATP
LPS+ATCC13124
LPS+CP1
LPS+CP3
pro-Caspase-1
Caspase-1 p20
pro-IL-1β
IL-1β p17
ASC
GADPH
Sup.
Lys.
E
IL-1β (pg/ml)
IL-18 (pg/ml)
WT
Nlrp3-/-
F
TNF-α (pg/ml)
G
%LDH release
H
KCL
GSDMD p53
GSDMD p30
I
-KCL
+KCL
J
K
L
P-MLKL
M
N
O
P
LPS+ATCC13124 LPS+ATP
LPS+CP1
LPS+CP3
R
S
Q
% of cells with ASC specks
Mlkl-/-
Nlrp3-/-
U
Bacterial Survival (Fold)
Mlkl-/-+rIL-18
V
Nlrp3-/-+rIL-18
W
Caspase-1/11-/-
Caspase-1/11-/-+rIL-18
T

Figure 5. Involvement of the NLRP3 inflammasome in MLKL-mediated host defense

WT and *Mlkl*$^{-/-}$ mice were intramuscularly infected with *C. perfringens* (1 × 10^7 CFU) for 24 h

(A) Representative muscle sections. *p*-MLKL (IHC) stained brown (upper panel, magnification ×100, lower panel, magnification, ×400). D-4-Amino-3-isoxazolidinone-pretreated WT and *Mlkl*$^{-/-}$ mice were orally infected with *C. perfringens* (1 × 10^8 CFU) for 24 h

(B and C) Representative duodenum and cecum sections. *p*-MLKL (IHC) stained brown (upper panel, magnification ×100, lower panel, magnification, ×200).

LPS-primed WT and *Nlrp3*$^{-/-}$ BMDMs were stimulated with ATP (5mM, 30min), *C. perfringens* strain ATCC13124, CP1 or CP3 (MOI = 20, 90 min).

(D) Cell supernatants and cell extracts immunoblotted for Caspase-1, IL-1β and ASC. GAPDH served as loading controls.

(E and F) Culture supernatants were analyzed for IL-1β, IL-18 and TNF-α by ELISA.

(G) LDH release was quantified to monitor cell lysis. Data are shown as the percentage of LDH release by Triton X-100 treated control cells.

(H) Cell supernatants and cell extracts immunoblotted for Caspase-1, GSDMD, IL-1β, ASC, and GAPDH.

(I and J) Culture supernatants were analyzed for IL-1β, IL-18, and TNF-α by ELISA.

(K) LDH release was quantified to monitor cell lysis. Data are shown as the percentage of LDH release by Triton X-100 treated control cells. LPS-primed WT and *Mlkl*$^{-/-}$ BMDMs were stimulated with ATP (5mM, 30min), *C. perfringens* strain ATCC13124, CP1, or CP3 (MOI = 20, 90 min).

(L) Cell supernatants and cell extracts immunoblotted for Caspase-1, GSDMD, IL-1β, ASC, *p*-MLKL, and GAPDH.

(M and N) Culture supernatants were analyzed for IL-1β, IL-18 and TNF-α by ELISA.

(O) LDH release was quantified to monitor cell lysis. Data are shown as the percentage of LDH release by Triton X-100 treated control cells. LPS-primed WT, *Mlkl*$^{-/-}$ and *Nlrp3*$^{-/-}$ BMDMs were stimulated with ATP (5mM, 30min), *C. perfringens* strain ATCC13124, CP1, or CP3 (MOI = 20, 90 min).

(P and Q) The cells were fixed, permeabilized, and stained for ASC (green). DAPI was used to label nuclei (blue). magnification, ×400. The percentage of cells containing ASC speckles was quantified. LPS-primed WT and *Mlkl*$^{-/-}$ BMDMs were stimulated with live bacteria (MOI = 20, 90 min), heat-killed bacteria (HK, MOI = 20, 90 min), bacterial culture supernatants (SN, 5 h) or bacterial α-toxin (20 μg/mL, 5 h).

(R and T) Culture supernatants were analyzed for IL-1β, IL-18, and TNF-α by ELISA.

(U–W) To determine the bacterial killing capacity of BMDMs, LPS-primed WT, *Mlkl*$^{-/-}$, *Nlrp3*$^{-/-}$, or *Caspase-1/11*$^{-/-}$ BMDMs were incubated with rIL-18 (1000 pg/mL) or PBS for 1 h before were infected with *C. perfringens* strain ATCC13124, CP1 or CP3 (MOI = 5) for 6 h, the supernatants were collected and plated on BHI agar plates to enumerate the bacteria after 24 h of anaerobic culture.

Graphs are means ± SD from data pooled from four to six (E, F, G, I, J, K, M, N, O, Q, R, S, T, U, V, and W) biological replicates. Data were considered significant when *$p < 0.05$ or **$p < 0.01$.

Mixed lineage kinase-like protein-mediated classical extracellular trap formation in response to *C. perfringens* is dependent on NLRP3 inflammasome signaling

To dissect the signaling mechanism that results in impaired extracellular traps formation upon *C. perfringens* infection in the absence of *Mlkl*, we assessed the raf-MEK-ERK signaling pathway, which was reported to regulate extracellular traps formation (Hakkim et al., 2011). However, the phosphorylation levels of P38, JNK, and ERK in both infected WT and infected *Mlkl*$^{-/-}$ macrophages were comparable (Figure 8A), indicating that MLKL-mediated extracellular traps release was not dependent on raf-MEK-ERK signaling. Recently, accumulating evidence has revealed that inflammasome signaling is associated with extracellular traps formation (Chen et al., 2018, 2021). To test whether NLRP3 inflammasome activation elicits MLKL-mediated classical extracellular traps release, LPS-primed BMDMs derived from WT, *Mlkl*$^{-/-}$, *Nlrp3*$^{-/-}$ or *Caspase-1/11*$^{-/-}$ mice were stimulated with *C. perfringens*, respectively. Interestingly, similar to *Mlkl*$^{-/-}$ macrophages, a significant decreased induction of extracellular traps formation was seen in *Nlrp3*$^{-/-}$ and *Caspase-1/11*$^{-/-}$ macrophages compared with WT macrophages (Figures 8B and 8C), as well as *Nlrp3* and *Caspase-1/11* deficiency also impaired *C. perfringens*-induced extracellular DNA release (Figure 8D). In addition, pretreatment with exogenous IL-18 could reverse the inhibitory effect of *Mlkl* deficiency on *C. perfringens*-triggered extracellular trap formation *in vitro* (Figures 8B–8D) and *in vivo* (Figures S3A and S3B). Therefore, these data suggested that MLKL-mediated extracellular trap formation in a NLRP3 inflammasome-dependent mechanism. In conclusion, these data establish that MLKL facilitates pathogen control via promoting NLRP3 inflammasome-extracellular traps axis as a defense response against *C. perfringens* infection.

DISCUSSION

Our uncover the unexpected finding that MLKL promotes bacterial killing and clearance by enhancing NLRP3 inflammasome-extracellular traps axis as a host defense against *C. perfringens* infection. Acting as a necroptosis effector, MLKL plays significant role in innate immunity. Recently, several studies including ours showed that MLKL is implicated in sensing pathogens infection (Kitur et al., 2016; Yu et al., 2018). However, little is known about the biological implications of MLKL in the infection of *C. perfringens*, an extracellular bacterial pathogen. *C. perfringens* infection usually begins suddenly and lasts for less than 24 h, thus, it is hard to detect early and treat timely, resulting in a huge burden to public health and animal husbandry worldwide. The development of new preventive and therapeutic strategies to combat *C. perfringens* infection has become more urgent. The host innate immune system provides the first line of defense for the early recognition and elimination of invading pathogens. Therefore, a detailed

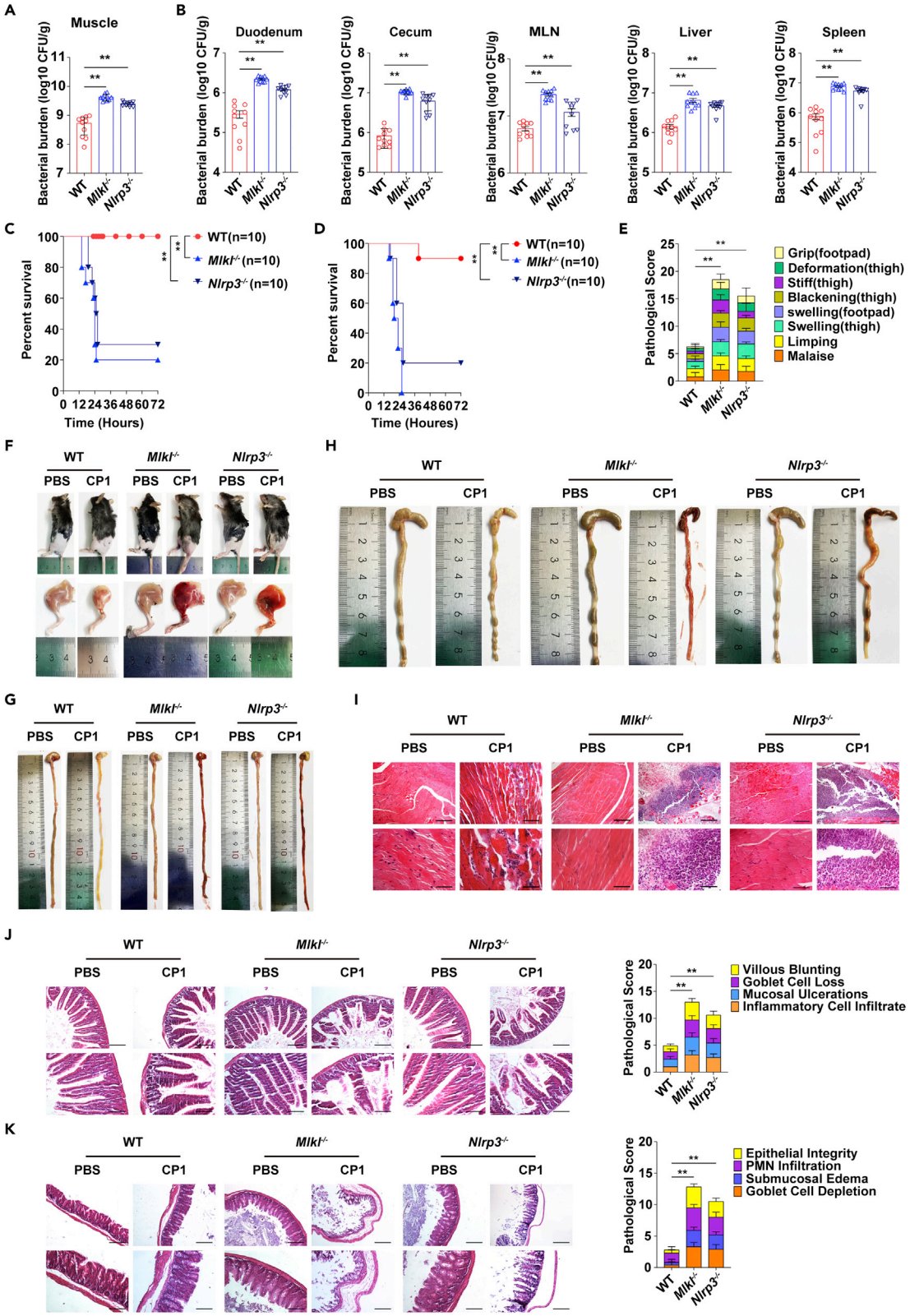
A
Muscle
Bacterial burden (log10 CFU/g)
B
Duodenum
Cecum
MLN
Liver
Spleen
WT
Mlkl-/-
Nlrp3-/-
C
Percent survival
WT(n=10)
Mlkl-/- (n=10)
Nlrp3-/- (n=10)
Time (Hours)
D
Time (Houres)
E
Pathological Score
Grip(footpad)
Deformation(thigh)
Stiff(thigh)
Blackening(thigh)
swelling(footpad)
Swelling(thigh)
Limping
Malaise
F
PBS
CP1
G
H
I
J
Villous Blunting
Goblet Cell Loss
Mucosal Ulcerations
Inflammatory Cell Infiltrate
K
Epithelial Integrity
PMN Infiltration
Submucosal Edema
Goblet Cell Depletion

Figure 6. *Nlrp3* deficiency attenuates bacterial clearance and impairs host defense against *C. perfringens* infection

Six to eight-weeks-old sex-matched WT, *Mlkl*$^{-/-}$, and *Nlrp3*$^{-/-}$ mice were intramuscularly infected with *C. perfringens*.

(A) Bacterial load in the muscle was detected (1 × 10^7 CFU, n = 10 each group, at 24 h p.i.).

(C) Survival (5 × 10^7 CFU, n = 10 each group).

(E) Cumulative gross pathology scores of infected mice (5 × 10^7 CFU, n = 10 each group).

(F) Representative pathologic photographs of the leg tissue of mice (1 × 10^7 CFU, n = 10 each group, at 24 h p.i.).

(I) Representative H&E staining of muscle tissue (1 × 10^7 CFU, n = 10 each group, at 24 h p.i., upper panel, magnification ×100, lower panel, magnification, ×400). Six to eight-weeks-old sex-matched WT, *Mlkl*$^{-/-}$, and *Nlrp3*$^{-/-}$ mice were orally infected with *C. perfringens*.

(B) Bacterial burden in the duodenum, cecum, MLN, liver, and spleen were quantitated (1 × 10^8 CFU, n = 10 each group, at 24 h p.i.).

(D) Survival (2 × 10^8 CFU, n = 10 each group).

(G and H) Representative gross appearance of duodenum and cecum (1 × 10^8 CFU, n = 10 each group, at 24 h p.i.).

(J and K) Representative H&E staining of duodenal and cecum tissue (1 × 10^8 CFU, n = 10 each group, at 24 h p.i., upper panel, magnification ×100, lower panel, magnification, ×200). Data were considered significant when **$p < 0.01$.

understanding of innate immunity in response to *C. perfringens* infection is critical for the design of potential therapeutic interventions.

Using *Mlkl*$^{-/-}$ mice, we initially demonstrate that MLKL promotes host survival and bacterial clearance during *C. perfringens* femoral muscle and mucosal infection, highlighting a novel role of MLKL in host defense against *C. perfringens* infection. To identify the potential mechanisms underlined MLKL-mediated defense, we set out to characterize the inflammasome signaling. *Mlkl* deficiency leads to inferior inflammasome activation in the muscle, duodenum, and cecum tissues during *C. perfringens* infection. Recent studies have shown that inflammasome activation participates in serious inflammatory diseases (Yu et al., 2015; Duewell et al., 2010; Wen et al., 2011) and is sufficient to protect the host against pathogens invading (Song-Zhao et al., 2014; Sellin et al., 2014). We hypothesized that the inflammasome signaling regulates MLKL-mediated host protection against *C. perfringens*. In line with our hypothesis, administration of exogenous IL-18 could rescue the susceptibility of *Mlkl*$^{-/-}$ mice to *C. perfringens* infection, reflected by remarkably alleviated organs damage and decreased bacteria colonization. Hence, it is quite possible that MLKL protects against *C. perfringens* infection by enhancing inflammasome activation.

Owing to MLKL mainly located in the recruited inflammatory cells, BMDMs were used to delve into the molecular mechanisms of MLKL-mediated inflammasome signaling. Increased evidence showed necroptotic stimuli-activated MLKL can promote NLRP3 inflammasome activation in a cell-intrinsic manner (Conos et al., 2017; Gutierrez et al., 2017). Although NLRP3 inflammasome can be initiated by *C. perfringens* (Yamamura et al., 2019), the understanding of regulatory mechanisms of NLRP3 inflammasome activation is limited. Consistent with this finding, we observed *Nlrp3* deficiency obviously restricts *C. perfringens*-triggered inflammasome signaling. To date, three mechanisms for NLRP3 inflammasome activation have been proposed (Bueter et al., 2014), including K^+ efflux (Munoz-Planillo et al., 2013), reactive oxygen species (ROS) generation (Zhou et al., 2011), and lysosomal destabilization (Hornung et al., 2008). Strikingly, we further found that *C. perfringens* elicits NLRP3 inflammasome activation in a K^+ efflux-dependent manner. Subsequently, we characterized whether MLKL modulates *C. perfringens*-stimulated K^+ efflux-dependent NLRP3 inflammasome activation. Consistent with *in vivo* data, *Mlkl* deficiency significantly impaired *C. perfringens*-induced inflammasome signaling via the NLRP3-ASC axis, demonstrated by eliminated Caspase-1, GSDMD, and IL-1β cleavages, decreased ASC speck formation, and reduced mature IL-1β and IL-18 release and LDH activity compared with WT macrophages. More importantly, *Mlkl*$^{-/-}$, *Nlrp3*$^{-/-}$, and *Caspase-1/11*$^{-/-}$ macrophages are unable to effectively control of multiplication of *C. perfringens*, and exogenous IL-18 treatment could rescue the defect in bacteria control. Used *Nlrp3*$^{-/-}$ mice, we further show that NLRP3 promotes host survival and bacterial clearance, and enhances host defense against *C. perfringens* infection. Thus, our *in vivo* and *in vitro* findings show that NLRP3 inflammasome is required for the protective effects of MLKL during bacterial infection. Interestingly, inflammasome signaling induced by bacterial α-toxin, heat-killed bacteria, or bacterial culture supernatants, was prominently inhibited in the absence of *Mlkl*, we suspect that active MLKL signaling may lead to enhancing the state of host immune response and limiting *C. perfringens* pathogenesis, although perfringolysin O (PFO), a key virulence factor of *C. perfringens*, was reported as an essential bacterial factor for triggering NLRP3 inflammasome activation (Yamamura et al., 2019). Although understanding the underlying mechanism of MLKL signaling and NLRP3 inflammasome signaling activation by *C. perfringens* awaits further investigation, this study extends our understanding of the biological implication of MLKL in host intrinsic immune responses.

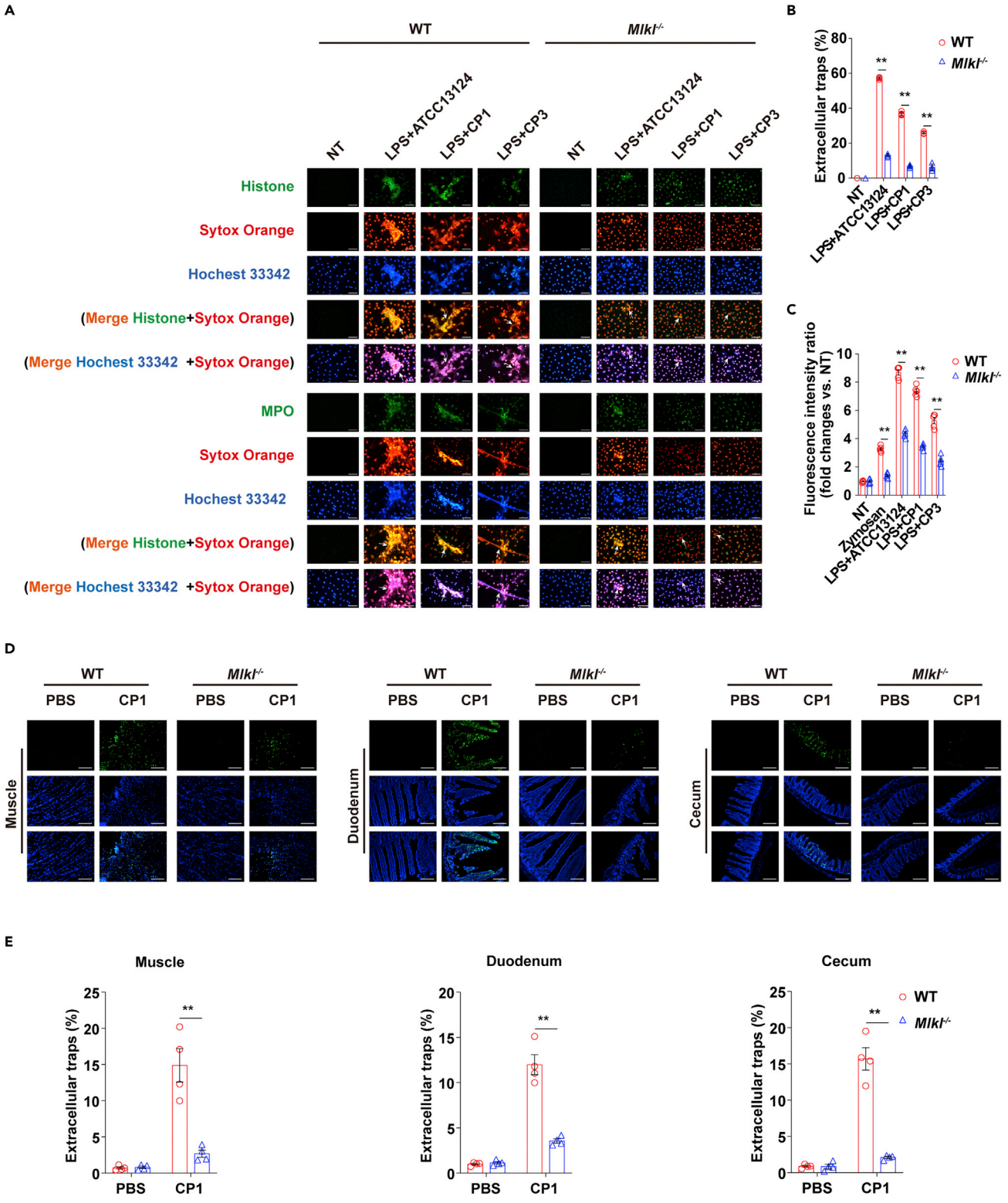

Figure 7. Extracellular traps formation contributes to MLKL-mediated host defense

LPS-primed WT and *Mlkl*$^{-/-}$ BMDMs were infected with *C. perfringens* strain ATCC13124, CP1, or CP3 (MOI = 20, 90 min).

(A) DNA decorated with histone and MPO within the extracellular traps structures was detected by immunofluorescence. Histone (green), MPO (green) and DNA (orange/blue). magnification, ×400.

Figure 7. *Continued*

(B) Macrophage extracellular traps were quantified using Fiji and expressed as the percentage of extracellular traps.

(C) The formation of bacteria-induced macrophage extracellular traps was quantified using Sytox Green. Cells stimulated with zymosan (1 mg/mL) were used as positive controls. WT and *Mlkl*$^{-/-}$ mice were intramuscularly infected with *C. perfringens* (1 × 10^7 CFU) for 24 h

(D and E) Representative muscle sections. Histone was analyzed by immunofluorescence (magnification, ×400), and extracellular traps were quantified using Fiji and expressed as the percentage of extracellular traps. D-4-Amino-3-isoxazolidinone-pretreated WT and *Mlkl*$^{-/-}$ mice were orally infected with *C. perfringens* (1 × 10^8 CFU) for 24 h

(D and E) Representative duodenum and cecum sections. Histone was analyzed by immunofluorescence (magnification, ×200), and extracellular traps were quantified using Fiji and expressed as the percentage of extracellular traps.

Graphs are means ± SD from data pooled from four to five (B, C, and E) biological replicates. Data were considered significant when $^{**}p < 0.01$. See also Figures S1 and S2.

Extracellular traps, a process by which innate myeloid cells such as neutrophils (Brinkmann et al., 2004), macrophages (Chow et al., 2010), basophils (Morshed et al., 2014), eosinophils (Yousefi et al., 2008), and mast cells (von Kockritz-Blickwede et al., 2008) kill invading pathogens, is the indispensable host intrinsic defense mechanism that differs from phagocytosis and degranulation. Activated innate myeloid cells release these web-like structures composed of decondensed chromatin and several bactericidal cellular proteins that provide extracellular sites for trapping and inhibiting a broad range of microorganisms. Meanwhile, we find that a defect in bacterial killing by impairing extracellular trap formation in macrophages and neutrophils. As MLKL is essential for the host defense against bacterial infection through enhancing bactericidal activity. We speculate whether MLKL also participates in the regulation of extracellular traps-dependent bacterial killing process. As expected, *Mlkl* deficiency significantly impaired *C. perfringens*-triggered extracellular traps release in macrophages and neutrophils. In line with this, a defect of extracellular traps formation was observed in bacteria-infected muscle, duodenum, and cecum tissues of *Mlkl*$^{-/-}$ mice. These data demonstrated that the protective effect of MLKL against *C. perfringens* infection is also dependent on the ability of MLKL to enhancing extracellular traps formation-mediated bacterial killing process.

Raf-MEK-ERK signaling has been proved to be required for several stimuli-elicited extracellular traps formation (Hakkim et al., 2011). Raf-MEK-ERK pathway is also induced by *C. perfringens*. We hypothesized that the defect of raf-MEK-ERK signaling may lead to impairing *C. perfringens*-triggered extracellular traps release in the absence of *Mlkl*. Unexpectedly, *Mlkl* deficiency does not impair *C. perfringens*-induced raf-MEK-ERK signaling, indicating that raf-MEK-ERK signaling is dispensable for MLKL-mediated extracellular traps formation. Recently, extracellular traps formation is driven by inflammasome-dependent IL-1β and IL-18 (Huang et al., 2020). Additionally, noncanonical inflammasome signaling can also elicit extracellular traps release via GSDMD activation (Chen et al., 2018). Here, we report a novel discovery of MLKL in the context of *C. perfringens* infection, which promotes classical extracellular trap formation in a NLRP3 inflammasome-dependent manner, in turn, enhances NLRP3 inflammasome-extracellular traps axis to strengthen bacterial control and host defense.

In summary, in the present study, we provide the first evidence demonstrating the importance of MLKL in mediating a protective innate immune response and preventing severe *C. perfringens* gas gangrene and enterocolitis. This information increases our understanding of the beneficial role of MLKL in host defense against *C. perfringens* infection. As master of key hub in enhancing the NLRP3 inflammasome-extracellular traps axis, MLKL improved host survival, induced the resolution of organs damage and inflammation, and accelerated bacterial eradication, supporting that it will be of interest to dissect whether pharmacological and vaccine activation of the MLKL-NLRP3 inflammasome-extracellular traps pathway confers protection in pathogens invading.

Limitations of the study

Our study provides an unexpected discovery of MLKL in the context of *C. perfringens* infection, which promotes NLRP3 inflammasome-extracellular traps axis to strengthen bacterial eradication and host defense. We provided a certain clue that NLRP3 inflammasome signaling is involved in MLKL-mediated extracellular traps formation, but the detailed downstream mechanism remains unclear. As MLKL is the critical terminal executioner of necroptosis, it is worthwhile to investigate the biological significance of necroptosis following *C. perfringens* infection in future studies. Also, our results showed that *C. perfringens* α-toxin may serve as an agonist of MLKL signaling. Although additional studies are needed to better explore the relationship between *C. perfringens* α-toxin and active MLKL signaling, and which is critical for the design of potential therapeutic interventions.

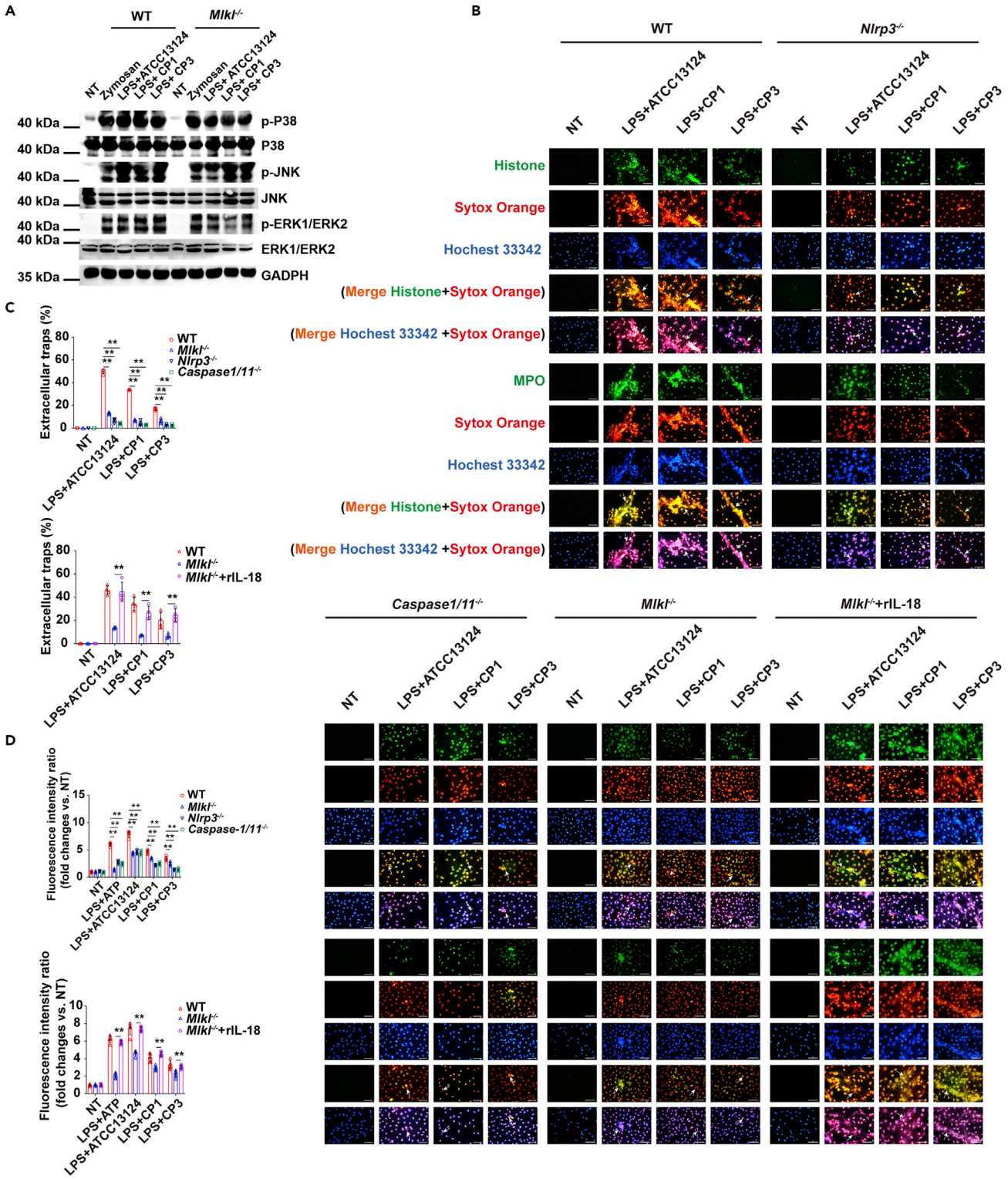

Figure 8. Blocking NLRP3 inflammasome signaling attenuates MLKL-mediated extracellular traps formation following *C. perfringens* challenge

LPS-primed WT and *Mlkl*$^{-/-}$ BMDMs were infected with *C. perfringens* strain ATCC13124, CP1, or CP3 (MOI = 20, 90 min).

(A) Cell extracts immunoblotted for p-P38, P38, *p*-JNK, JNK, *p*-ERK1/ERK2, ERK1/ERK2, and GAPDH. Cells stimulated with zymosan (1 mg/mL) were used as positive controls. LPS-primed WT, *Mlkl*$^{-/-}$, *Nlrp3*$^{-/-}$, and *Caspase-1/11*$^{-/-}$ BMDMs were treated with or without rIL-18 (1000 pg/mL) for 1 h before were infected with *C. perfringens* strain ATCC13124, CP1 or CP3 (MOI = 20, 90 min).

Figure 8. *Continued*

(B) DNA decorated with histone and MPO within the extracellular traps structures were detected by immunofluorescence. Histone (green), MPO (green) and DNA (orange/blue). magnification, ×400.

(C) Macrophage extracellular traps were quantified using Fiji and expressed as the percentage of extracellular traps.

(D) The formation of bacteria-induced macrophage extracellular traps was quantified using Sytox Green. Cells stimulated with ATP (5 mM, 30 min) were used as positive controls.

Graphs are means ± SD from data pooled from four to five (C and D) biological replicates. NT: Untreated cells. Data were considered significant when $^{**}p < 0.01$. See also Figure S3.

ETHICS STATEMENT

All animal studies were conducted according to experimental practices and standards approved by the Animal Welfare and Research Ethics Committee at Inner Mongolia University ([2020] 022).

STAR★METHODS

Detailed methods are provided in the online version of this paper and include the following:

- KEY RESOURCES TABLE
- RESOURCE AVAILABILITY
  - Lead contact
  - Materials availability
  - Data and code availability
- EXPERIMENTAL MODEL AND SUBJECT DETAILS
  - Mice
  - Cell lines
  - *C. perfringens* strain CP1 for establishment of a mouse model of gas gangrene
  - Enterocolitis model
- METHOD DETAILS
  - Administration of recombinant IL-18
  - Inflammasome assays
  - Extracellular traps formation assays
  - Tissue histology and immunostaining
  - Cytokine release analysis
  - Real-time PCR
  - Immunoblotting
- QUANTIFICATION AND STATISTICAL ANALYSIS

SUPPLEMENTAL INFORMATION

Supplemental information can be found online at https://doi.org/10.1016/j.isci.2022.105121.

ACKNOWLEDGMENTS

This work was supported by The National Natural Science Foundation of China [No. 32160832], Natural Science Foundation of Inner Mongolia Autonomous Region of China [No. 2021BS03003], Research Program of Science and Technology at Universities of Inner Mongolia Autonomous Region of China [No. NJZZ21001], Program for Young Talents of Science and Technology in Universities of Inner Mongolia Autonomous Region of China [No. NJYT22104], Provincial University Student Innovation and Entrepreneurship Training Programs of Inner Mongolia University [No. 21400-121081/031], Science and Technology Major Project of Inner Mongolia Autonomous Region of China to the State Key Laboratory of Reproductive Regulation and Breeding of Grassland Livestock [No. zdzx2018065], Inner Mongolia University Startup Foundation for Advanced Talents [No. 30500-5185139].

AUTHOR CONTRIBUTIONS

Y.L., L.-H.X., and S.-X.Y. designed experiments. Y.L., L.-H.X., F.-X.L., N.W., Y.-Z.M., J.-W.L., Y.-J.W., J.L., Y.-X.L., X.-Y.W., and F.-H.M. performed the experiments and analyzed the data. Y.L. wrote the article. Y.-J.Y., G.-P.L., X.W., and S.-X.Y. revised the article. All authors read and approved the final article.

DECLARATION OF INTERESTS

The authors declare no competing interests.

INCLUSION AND DIVERSITY

We worked to ensure sex balance in the selection of non-human subjects.

We worked to ensure diversity in experimental samples through the selection of the cell lines.

We worked to ensure diversity in experimental samples through the selection of genomic datasets.

While citing references scientifically relevant for this work, we also actively worked to promote gender balance in our reference list.

Received: November 12, 2021
Revised: July 16, 2022
Accepted: September 7, 2022
Published: October 21, 2022

REFERENCES

Ahrenholz, D.H. (1988). Necrotizing soft-tissue infections. Surg. Clin. North Am. *68*, 199–214. https://doi.org/10.1016/S0039-6109(16)44440-3.

Asaka, D., Nakajima, T., Ohno, T., Matsuwaki, Y., Moriyama, H., and Saito, H. (2009). Reciprocal regulation of chitinase 3-like1 production from human macrophages by Th1 and Th2 cytokines. J. Allergy Clin. Immunol. *123*, S255. https://doi.org/10.1016/j.jaci.2008.12.987.

Awad, M.M., Ellemor, D.M., Boyd, R.L., Emmins, J.J., and Rood, J.I. (2001). Synergistic effects of alpha-toxin and perfringolysin O in *Clostridium perfringens*-mediated gas gangrene. Infect. Immun. *69*, 7904–7910. https://doi.org/10.1128/IAI.69.12.7904-7910.2001.

Brinkmann, V., Reichard, U., Goosmann, C., Fauler, B., Uhlemann, Y., Weiss, D.S., Weinrauch, Y., and Zychlinsky, A. (2004). Neutrophil extracellular traps kill bacteria. Science *303*, 1532–1535. https://doi.org/10.1126/science.1092385.

Bueter, C.L., Lee, C.K., Wang, J.P., Ostroff, G.R., Specht, C.A., and Levitz, S.M. (2014). Spectrum and mechanisms of inflammasome activation by chitosan. J. Immunol. *192*, 5943–5951. https://doi.org/10.4049/jimmunol.1301695.

Chen, K.W., Monteleone, M., Boucher, D., Sollberger, G., Ramnath, D., Condon, N.D., von Pein, J.B., Broz, P., Sweet, M.J., and Schroder, K. (2018). Noncanonical inflammasome signaling elicits gasdermin D-dependent neutrophil extracellular traps. Sci. Immunol. *3*, eaar6676. https://doi.org/10.1126/sciimmunol.aar6676.

Chen, W., Yu, S.X., Zhou, F.H., Zhang, X.J., Gao, W.Y., Li, K.Y., Liu, Z.Z., Han, W.Y., and Yang, Y.J. (2019). DNA sensor IFI204 contributes to host defense against Staphylococcus aureus infection in mice. Front. Immunol. *10*, 474. https://doi.org/10.3389/fimmu.2019.00474.

Chen, W., Zhao, J., Mu, D., Wang, Z., Liu, Q., Zhang, Y., and Yang, D. (2021). Pyroptosis mediates neutrophil extracellular trap formation during bacterial infection in zebrafish. J. Immunol. *206*, 1913–1922. https://doi.org/10.4049/jimmunol.2001335.

Chow, O.A., von Köckritz-Blickwede, M., Bright, A.T., Hensler, M.E., Zinkernagel, A.S., Cogen, A.L., Gallo, R.L., Monestier, M., Wang, Y., Glass, C.K., et al. (2010). Statins enhance formation of phagocyte extracellular traps. Cell Host Microbe *8*, 445–454. https://doi.org/10.1016/j.chom.2010.10.005.

Chudnovskiy, A., Mortha, A., Kana, V., Kennard, A., Ramirez, J.D., Rahman, A., Remark, R., Mogno, I., Ng, R., Gnjatic, S., et al. (2016). Host-Protozoan interactions protect from mucosal infections through activation of the inflammasome. Cell *167*, 444–456.e14. https://doi.org/10.1016/j.cell.2016.08.076.

Conos, S.A., Chen, K.W., De Nardo, D., Hara, H., Whitehead, L., Núñez, G., Masters, S.L., Murphy, J.M., Schroder, K., Vaux, D.L., et al. (2017). Active MLKL triggers the NLRP3 inflammasome in a cell-intrinsic manner. Proc. Natl. Acad. Sci. USA *114*, E961–E969. https://doi.org/10.1073/pnas.1613305114.

Duewell, P., Kono, H., Rayner, K.J., Sirois, C.M., Vladimer, G., Bauernfeind, F.G., Abela, G.S., Franchi, L., Nuñez, G., Schnurr, M., et al. (2010). NLRP3 inflammasomes are required for atherogenesis and activated by cholesterol crystals. Nature *464*, 1357–1361. https://doi.org/10.1038/nature08938.

Erben, U., Loddenkemper, C., Doerfel, K., Spieckermann, S., Haller, D., Heimesaat, M.M., Zeitz, M., Siegmund, B., and Kühl, A.A. (2014). A guide to histomorphological evaluation of intestinal inflammation in mouse models. Int. J. Clin. Exp. Pathol. *7*, 4557–4576.

Grass, J.E., Gould, L.H., and Mahon, B.E. (2013). Epidemiology of foodborne disease outbreaks caused by Clostridium perfringens, United States, 1998–2010. Foodborne Pathog. Dis. *10*, 131–136. https://doi.org/10.1089/fpd.2012.1316.

Groß, C.J., Mishra, R., Schneider, K.S., Médard, G., Wettmarshausen, J., Dittlein, D.C., Shi, H., Gorka, O., Koenig, P.A., Fromm, S., et al. (2016). K(+) efflux-independent NLRP3 inflammasome activation by small molecules targeting mitochondria. Immunity *45*, 761–773. https://doi.org/10.1016/j.immuni.2016.08.010.

Gutierrez, K.D., Davis, M.A., Daniels, B.P., Olsen, T.M., Ralli-Jain, P., Tait, S.W.G., Gale, M., Jr., and Oberst, A. (2017). MLKL activation triggers NLRP3-mediated processing and release of IL-1beta independently of gasdermin-D. J. Immunol. *198*, 2156–2164. https://doi.org/10.4049/jimmunol.1601757.

Hakkim, A., Fuchs, T.A., Martinez, N.E., Hess, S., Prinz, H., Zychlinsky, A., and Waldmann, H. (2011). Activation of the Raf-MEK-ERK pathway is required for neutrophil extracellular trap formation. Nat. Chem. Biol. *7*, 75–77. https://doi.org/10.1038/nchembio.496.

Hornung, V., Bauernfeind, F., Halle, A., Samstad, E.O., Kono, H., Rock, K.L., Fitzgerald, K.A., and Latz, E. (2008). Silica crystals and aluminum salts activate the NALP3 inflammasome through phagosomal destabilization. Nat. Immunol. *9*, 847–856. https://doi.org/10.1038/ni.1631.

Huang, W., Jiao, J., Liu, J., Huang, M., Hu, Y., Ran, W., Yan, L., Xiong, Y., Li, M., Quan, Z., et al. (2020). MFG-E8 accelerates wound healing in diabetes by regulating "NLRP3 inflammasome-neutrophil extracellular traps" axis. Cell Death Discov. *6*, 84. https://doi.org/10.1038/s41420-020-00318-7.

Huang, X.Y., Sun, W.Y., Yan, Z.Q., Shi, H.R., Yang, Q.L., Wang, P.F., Li, S.G., Liu, L.X., Zhao, S.G., and Gun, S.B. (2019). Novel insights reveal anti-microbial gene regulation of piglet intestine immune in response to Clostridium perfringens infection. Sci. Rep. *9*, 1963. https://doi.org/10.1038/s41598-018-37898-5.

Kitur, K., Wachtel, S., Brown, A., Wickersham, M., Paulino, F., Peñaloza, H.F., Soong, G., Bueno, S., Parker, D., and Prince, A. (2016). Necroptosis promotes Staphylococcus aureus clearance by inhibiting excessive inflammatory signaling. Cell Rep. *16*, 2219–2230. https://doi.org/10.1016/j.celrep.2016.07.039.

Lee, A., May, A., and Obremskey, W.T. (2019). Necrotizing soft-tissue infections: an orthopaedic emergency. J. Am. Acad. Orthop. Surg. *27*, e199–e206. https://doi.org/10.5435/jaaos-d-17-00616.

Lei, Q.-Q., Hu, G.-Q., Chen, W., Yu, S.-X., Qi, S., Du, C.-T., Gu, J.-M., Lin, T.-J., and Yang, Y.-J. (2016). RCAN1 deficiency protects against Salmonella intestinal infection by modulating JNK activation. Mol. Immunol. *77*, 26–33. https://doi.org/10.1016/j.molimm.2016.07.009.

Mathur, R., Oh, H., Zhang, D., Park, S.-G., Seo, J., Koblansky, A., Hayden, M.S., and Ghosh, S. (2012). A mouse model of Salmonella typhi infection. Cell *151*, 590–602. https://doi.org/10.1016/j.cell.2012.08.042.

McComb, S., Cessford, E., Alturki, N.A., Joseph, J., Shutinoski, B., Startek, J.B., Gamero, A.M., Mossman, K.L., and Sad, S. (2014). Type-I interferon signaling through ISGF3 complex is required for sustained Rip3 activation and necroptosis in macrophages. Proc. Natl. Acad. Sci. USA *111*, E3206–E3213. https://doi.org/10.1073/pnas.1407068111.

Morshed, M., Hlushchuk, R., Simon, D., Walls, A.F., Obata-Ninomiya, K., Karasuyama, H., Djonov, V., Eggel, A., Kaufmann, T., Simon, H.U., et al. (2014). NADPH oxidase-independent formation of extracellular DNA traps by basophils. J. Immunol. *192*, 5314–5323. https://doi.org/10.4049/jimmunol.1303418.

Munoz-Planillo, R., Kuffa, P., Martínez-Colón, G., Smith, B.L., Rajendiran, T.M., and Núñez, G. (2013). K(+) efflux is the common trigger of NLRP3 inflammasome activation by bacterial toxins and particulate matter. Immunity *38*, 1142–1153. https://doi.org/10.1016/j.immuni.2013.05.016.

Petrie, E.J., Sandow, J.J., Jacobsen, A.V., Smith, B.J., Griffin, M.D.W., Lucet, I.S., Dai, W., Young, S.N., Tanzer, M.C., Wardak, A., et al. (2018). Conformational switching of the pseudokinase domain promotes human MLKL tetramerization and cell death by necroptosis. Nat. Commun. *9*, 2422. https://doi.org/10.1038/s41467-018-04714-7.

Rathinam, V.A.K., Zhao, Y., and Shao, F. (2019). Innate immunity to intracellular LPS. Nat. Immunol. *20*, 527–533. https://doi.org/10.1038/s41590-019-0368-3.

Roesner, L.M., Ernst, M., Chen, W., Begemann, G., Kienlin, P., Raulf, M.K., Lepenies, B., and Werfel, T. (2019). Human thioredoxin, a damage-associated molecular pattern and Malassezia-crossreactive autoallergen, modulates immune responses via the C-type lectin receptors Dectin-1 and Dectin-2. Sci. Rep. *9*, 11210. https://doi.org/10.1038/s41598-019-47769-2.

Schindelin, J., Arganda-Carreras, I., Frise, E., Kaynig, V., Longair, M., Pietzsch, T., Preibisch, S., Rueden, C., Saalfeld, S., Schmid, B., et al. (2012). Fiji: an open-source platform for biological-image analysis. Nat. Methods *9*, 676–682. https://doi.org/10.1038/nmeth.2019.

Sellin, M.E., Müller, A.A., Felmy, B., Dolowschiak, T., Diard, M., Tardivel, A., Maslowski, K.M., and Hardt, W.D. (2014). Epithelium-intrinsic NAIP/NLRC4 inflammasome drives infected enterocyte expulsion to restrict Salmonella replication in the intestinal mucosa. Cell Host Microbe *16*, 237–248. https://doi.org/10.1016/j.chom.2014.07.001.

Sisquella, X., Ofir-Birin, Y., Pimentel, M.A., Cheng, L., Abou Karam, P., Sampaio, N.G., Penington, J.S., Connolly, D., Giladi, T., Scicluna, B.J., et al. (2017). Malaria parasite DNA-harbouring vesicles activate cytosolic immune sensors. Nat. Commun. *8*, 1985. https://doi.org/10.1038/s41467-017-02083-1.

Song-Zhao, G.X., Srinivasan, N., Pott, J., Baban, D., Frankel, G., and Maloy, K.J. (2014). Nlrp3 activation in the intestinal epithelium protects against a mucosal pathogen. Mucosal Immunol. *7*, 763–774. https://doi.org/10.1038/mi.2013.94.

Tanzer, M.C., Matti, I., Hildebrand, J.M., Young, S.N., Wardak, A., Tripaydonis, A., Petrie, E.J., Mildenhall, A.L., Vaux, D.L., Vince, J.E., et al. (2016). Evolutionary divergence of the necroptosis effector MLKL. Cell Death Differ. *23*, 1185–1197. https://doi.org/10.1038/cdd.2015.169.

Thurston, T.L.M., Matthews, S.A., Jennings, E., Alix, E., Shao, F., Shenoy, A.R., Birrell, M.A., and Holden, D.W. (2016). Growth inhibition of cytosolic Salmonella by caspase-1 and caspase-11 precedes host cell death. Nat. Commun. *7*, 13292. https://doi.org/10.1038/ncomms13292.

Tourlomousis, P., Wright, J.A., Bittante, A.S., Hopkins, L.J., Webster, S.J., Bryant, O.J., Mastroeni, P., Maskell, D.J., and Bryant, C.E. (2020). Modifying bacterial flagellin to evade Nod-like Receptor CARD 4 recognition enhances protective immunity against Salmonella. Nat. Microbiol. *5*, 1588–1597. https://doi.org/10.1038/s41564-020-00801-y.

von Kockritz-Blickwede, M., Goldmann, O., Thulin, P., Heinemann, K., Norrby-Teglund, A., Rohde, M., and Medina, E. (2008). Phagocytosis-independent antimicrobial activity of mast cells by means of extracellular trap formation. Blood *111*, 3070–3080. https://doi.org/10.1182/blood-2007-07-104018.

Wen, H., Gris, D., Lei, Y., Jha, S., Zhang, L., Huang, M.T.-H., Brickey, W.J., and Ting, J.P.Y. (2011). Fatty acid–induced NLRP3-ASC inflammasome activation interferes with insulin signaling. Nat. Immunol. *12*, 408–415. https://doi.org/10.1038/ni.2022.

Wu, J., Huang, Z., Ren, J., Zhang, Z., He, P., Li, Y., Ma, J., Chen, W., Zhang, Y., Zhou, X., et al. (2013). Mlkl knockout mice demonstrate the indispensable role of Mlkl in necroptosis. Cell Res. *23*, 994–1006. https://doi.org/10.1038/cr.2013.91.

Yamamura, K., Ashida, H., Okano, T., Kinoshita-Daitoku, R., Suzuki, S., Ohtani, K., Hamagaki, M., Ikeda, T., and Suzuki, T. (2019). Inflammasome activation induced by perfringolysin O of Clostridium perfringens and its involvement in the progression of gas gangrene. Front. Microbiol. *10*, 2406. https://doi.org/10.3389/fmicb.2019.02406.

Yousefi, S., Gold, J.A., Andina, N., Lee, J.J., Kelly, A.M., Kozlowski, E., Schmid, I., Straumann, A., Reichenbach, J., Gleich, G.J., et al. (2008). Catapult-like release of mitochondrial DNA by eosinophils contributes to antibacterial defense. Nat. Med. *14*, 949–953. https://doi.org/10.1038/nm.1855.

Yu, S.-X., Chen, W., Liu, Z.-Z., Zhou, F.-H., Yan, S.-Q., Hu, G.-Q., Qin, X.-X., Zhang, J., Ma, K., Du, C.-T., et al. (2018). Non-hematopoietic MLKL protects against Salmonella mucosal infection by enhancing inflammasome activation. Front. Immunol. *9*, 119. https://doi.org/10.3389/fimmu.2018.00119.

Yu, S.-X., Du, C.-T., Chen, W., Lei, Q.-Q., Li, N., Qi, S., Zhang, X.-J., Hu, G.-Q., Deng, X.-M., Han, W.-Y., et al. (2015). Genipin inhibits NLRP3 and NLRC4 inflammasome activation via autophagy suppression. Sci. Rep. *5*, 17935. https://doi.org/10.1038/srep17935.

Yu, S.-X., Zhou, F.-H., Chen, W., Jiang, G.-M., Du, C.-T., Hu, G.-Q., Liu, Z.-Z., Yan, S.-Q., Gu, J.-M., Deng, X.-M., et al. (2017). Decidual stromal cell necroptosis contributes to polyinosinic-polycytidylic acid-triggered abnormal murine pregnancy. Front. Immunol. *8*, 916. https://doi.org/10.3389/fimmu.2017.00916.

Zhivaki, D., and Kagan, J.C. (2021). Innate immune detection of lipid oxidation as a threat assessment strategy. Nat. Rev. Immunol. *22*, 322–330. https://doi.org/10.1038/s41577-021-00618-8.

Zhou, R., Yazdi, A.S., Menu, P., and Tschopp, J. (2011). A role for mitochondria in NLRP3 inflammasome activation. Nature *469*, 221–225. https://doi.org/10.1038/nature09663.

STAR★METHODS

KEY RESOURCES TABLE

REAGENT or RESOURCE	SOURCE	IDENTIFIER
Antibodies		
Anti-ASC	Adipogen	Cat # A29151803f
Alexa Fluor® 488-conjugated anti-rabbit IgG secondary antibody	Abcam	Cat # ab150077
Anti-MPO	Biorbyt	Cat # orb16003; RRID: AB_10752135
Anti-ELANE	ABclonal	Cat # A13015; RRID: AB_2759862
Anti-histone	ABclonal	Cat # A2348
Anti-Ly-6G/Ly-6c	BioLegend	Cat # 108419; RRID: AB_493480
Anti-F4/80	BioLegend	Cat # 123119; RRID: AB_893491
Anti-mucin 2	Santa Cruz	Cat # sc-515032; RRID: AB_2815005
Anti-claudin 3	Abcam	Cat # A2946
Anti-p-MLKL	Abcam	Cat # ab196436
Anti-Caspase-1	Adipogen	Cat # A28881708
Anti-IL-1β	Adipogen	Cat # PRP1119
Anti-GSDMD	Santa Cruz	Cat # sc-393656
Anti-P38 MAPK	ABclonal	Cat # A4771; RRID: AB_2863345
Anti-p-P38 MAPK	ABclonal	Cat # AP0526
Anti-JNK	Proteintech	Cat # 66210-1-lg
Anti-p-JNK	ABclonal	Cat # AP0276
Anti-ERK1/2	ABclonal	Cat # A10613
Anti-p-ERK1/2	ABclonal	Cat # AP0472
Anti-GADPH	Roteintech	Cat # 60004-1-lg
Bacterial and virus strains		
C. perfringens strain ATCC13124	Guangdong Huankai Microbial Sci.&Tech.CO.,Ltd	FSCC137003
C. perfringens strain CP1	This paper	NCBI GenBank: MW440585
C. perfringens strain CP3	This paper	NCBI GenBank: MW440587
Chemicals, peptides, and recombinant proteins		
RPMI1640 medium	Gibco	Cat # 31800-022
FBS fetal bovine serum	Gibco	Cat # A31608-02
Penicillin	Gibco	Cat # 15140-122
Streptomycins	Gibco	Cat # 15140-122
D-4-Amino-3-isoxazolidinone	Coolaber	Cat # CA1662
Recombinant IL-18	Novoprotein	Cat # CK06
LPS	Invivogen,	Cat # tlrl-3pelps
Potassium chloride	Sigma-Aldrich	Cat # 1049360250
ATP	Sigma	Cat # A2383
DAPI	Solarbio	Cat # C0065
Sytox Orange	Invitrogen	Cat # S-11368
Hoechst 33342	Wanleibio	Cat # WLA042a
Sytox Green	Invitrogen	Cat # S7020
Formalin solution	Macklin	Cat # P804536

(*Continued on next page*)

Continued

REAGENT or RESOURCE	SOURCE	IDENTIFIER
Hematoxylin & eosin	Solarbio	Cat # SL7050-500
Triton X-100	Sigma-Aldrich	Cat # 93443
Complete protease inhibitor cocktail	Sigma-Aldrich	Cat # 9036-19-5
TRI-reagent	Sigma-Aldrich	Cat # T9424
SYBR Green	Roche	Cat # 04913914001
Tris-HCl	Sigma-Aldrich	Cat #10812846001
NaCl	Sigma-Aldrich	Cat # S3014
Na_3VO_4	Sigma-Aldrich	Cat #S 6508
Critical commercial assays		
Mouse bone marrow neutrophils isolation kit ®	TianJin 371 HaoYang Biological Manufacture Co	Cat # LZS1100
AB-PAS Stain Kit	Solarbio,	Cat # 1285
LDH Cytotoxicity Assay kit®	Beyotime Biotechnology	Cat # C0017
TUNEL staining kit	KeyGEN BioTECH	Cat # KGA7061
TNF-α ELISA Kit	R&D	Cat # MTA00B
IL-1β ELISA Kit	R&D	Cat # MLB00C
IL-18 ELISA Kit	Solarbio	Cat # SEKM-0019
BCA Protein Quantification Kit	Thermo	Cat # 23225
Experimental models: Cell lines		
Mouse BMDM	This paper	N/A
Mouse bone marrow-derived neutrophils	This paper	N/A
Experimental models: Organisms/strains		
Mouse: Wildtype:C57BL/6J	Jackson Laboratory	Strain #:000664 RRID:IMSR_JAX:000664
Mouse: *Mlkl*$^{-/-}$	(Wu et al., 2013) Gift by Dr. Jia-Huai Han (Xiamen University, China)	N/A
Mouse: *Nlrp3*$^{-/-}$	Jackson Laboratory	Strain #:021302 RRID:IMSR_JAX:021302
Mouse: *Caspase1/11*$^{-/-}$	(Thurston et al., 2016) Gift by Dr. Feng Shao (National Institute of Biological Sciences, Beijing, China)	N/A
Oligonucleotides		
GADPH-F: CACCCCAGCAAGGACACTGAGCAAG	This paper	N/A
GADPH-R: GGGGGTCTGGGATGGAAATTGTGAG	This paper	N/A
Occludin-F: CAGCCTTCTGCTTCATCG	This paper	N/A
Occludin-R: GTCGGGTTCACTCCCATTA	This paper	N/A
ZO-1-F: GACCTTGAGCAGCCGTCATA	This paper	N/A
ZO-1-R: CCGTAGGCGATGGTCATAGTT	This paper	N/A
Claudin 3-F: CCTAGGAACTGTCCAAGCCG	This paper	N/A
Claudin 3-R: CCC- GTTTCATGGTTTGCCTG	This paper	N/A
Software and algorithms		
Prism9	GraphPad Software	https://www.graphpad.com/
ImageJ(Fiji)	(Schindelin et al., 2012)	https://fiji.sc

RESOURCE AVAILABILITY

Lead contact

Further information and requests for data should be directed to and will be fulfilled by the lead contact, Shui-Xing Yu (shuixingyu@imu.edu.cn).

Materials availability

This study did not generate new materials or reagents.

Data and code availability

- Information on the *C. perfringens* clinical isolates have been deposited in NCBI GenBank and are publicly available as of the date of publication. Accession numbers are listed in the key resources table. All data produced or analyzed for this study are included in the published article and its supplementary files, and will be shared by the lead contact upon request.
- This paper does not report original code.
- Any additional information required to reanalyze the data reported in this work paper is available from the lead contact upon request.

EXPERIMENTAL MODEL AND SUBJECT DETAILS

Mice

Mlkl$^{-/-}$ mice were a gift from Dr. Jia-Huai Han (Xiamen University, China) (Wu et al., 2013). *Nlrp3*$^{-/-}$ mice (Jackson Laboratory, Strain #:021302 RRID: IMSR_JAX:021302) were purchased from The Jackson Laboratory (Bar Harbor, ME, USA). *Caspase-1/11*$^{-/-}$ mice were kindly provided by Dr. Feng Shao (National Institute of Biological Sciences, Beijing, China) (Thurston et al., 2016). They were subsequently backcrossed onto the C57BL/6J (Jackson Laboratory, Strain #:000664 RRID: IMSR_JAX:000664) background for eight generations and heterozygous breeding pairs were used to generate WT mice. The mice were housed in a pathogen-free facility, with sterile food and water in the animal house of the Laboratory Animal Center of Inner Mongolia University. All animal studies were conducted according to the experimental practices and standards approved by the Animal Welfare and Research Ethics Committee at Inner Mongolia University ([2020]022).

Cell lines

Bone marrow-derived macrophages (BMDMs) were prepared and cultured as previously described (Yu et al., 2015). In brief, BMDMs were isolated from mouse femurs of six to eight weeks old mice and cultured in RPMI1640 medium (Gibco, #31800-022) containing 10% FBS fetal bovine serum (Gibco, #A31608-02), 25% L929 cell–conditioned medium, 100 U/mL penicillin (Gibco, #15140-122), and 100 U/mL streptomycins (Gibco, #15140-122), at 37°C in a humidified atmosphere containing 5% CO_2. Matured BMDMs were harvested for assays at day 7 of differentiation. Neutrophils were isolated by using the commercially available mouse bone marrow neutrophils isolation kit® (TianJin HaoYang Biological Manufacture Co., #LZS1100, China) according to the manufacturer's instructions.

C. perfringens strain CP1 for establishment of a mouse model of gas gangrene

For the gas gangrene model, representative *C. perfringens* strain CP1 (a clinical isolate of *C. perfringens*, specific 16S rDNA gene sequence data deposited at NCBI GenBank: MW440585) was grown to exponential phase in brain heart infusion broth (BHI, Qingdao Hi-Tech Industrial Park Haibo Biotechnology Co., Ltd, #HB8297-5, China) under anaerobic conditions at 37°C. Six to eight weeks old sex-matched mice were intramuscularly infected with 1×10^7 colony-forming units (CFUs) of *C. perfringens* strain CP1 diluted in PBS in a total volume of 100 μL. At 24 h p.i., mice were euthanized to collect infected leg muscle for quantification of bacterial burden. For the survival study, mice were intramuscularly challenged with 5×10^7 CFUs of *C. perfringens* strain CP1. *C. perfringens* gas gangrene was assessed in a blinded manner using an amended version of a previously described scoring criteria (Awad et al., 2001). In brief, the severity of grip, deformation, stiffness, blackening, swelling, limping, and malaise pathology parameters were scored as either 0 (no discernible pathology), 0.5 (some demonstrable pathology), 1 (mild pathology), 1.5 (clearly noticeable pathological changes), 2 (moderate pathology), 2.5 (marked pathology apparent) or 3 (near death).

Enterocolitis model

To induce enterocolitis, following the administration of 0.4 mg of D-4-Amino-3-isoxazolidinone (Coolaber, #CA1662) per mouse, six to eight weeks old sex-matched mice were orally challenged with 1×10^8 CFUs of representative *C. perfringens* strain CP1 diluted in PBS in a total volume of 100 μL. At 24 h p.i., mice were euthanized to collect duodenum, cecum, spleen, liver, and MLN for quantification of bacterial burden. Tissue samples of duodenum and cecum were fixed in buffered formalin solution (4%) and embedded in paraffin. Sections (5 μm thick) were then stained with hematoxylin and eosin (H&E, Solarbio, #SL7050-500). *C. perfringens*-induced enterocolitis was assessed in a blinded manner using an amended version of a previously described score (Erben et al., 2014; Lei et al., 2016). In brief, duodenum histopathology scores for damage were determined as follows: inflammatory cell infiltrate (scores 0 to 4), mucosal ulcerations (scores 0 to 4), goblet cell loss (scores 0 to 4) and villous blunting (scores 0 to 4). Cecum pathology scores were determined as follows: submucosal edema (scores 0 to 3), goblet cell depletion (scores 0 to 3), epithelial integrity (scores 0 to 3), and polymorphonuclear leukocyte (PMN) infiltration (scores 0 to 4). For the survival study, mice were orally infected with 2×10^8 CFUs and 1×10^8 CFUs of *C. perfringens* strain CP1, respectively.

METHOD DETAILS

Administration of recombinant IL-18

Mlkl$^{-/-}$ mice were i.p. injected recombinant IL-18 (Novoprotein, #CK06) at a dose of 1.0 μg per mouse in 100 μL PBS on day-1 and day 0. The mice were intramuscularly or orally infected with 1×10^7 or 1×10^8 CFUs of representative *C. perfringens* strain CP1 on day 0. At 24 h p.i., tissue samples of muscle, duodenum and cecum were fixed in 4% neutral buffered formalin and sections were stained with H&E to examine morphologic changes. Meanwhile, aseptically excised tissues were homogenized mechanically in cold PBS (at a ratio of 4 mL per gram tissue). Serial dilutions of tissue homogenates were plated on agar plates and Log CFUs per organ was determined after 24 h of anaerobic culture.

Inflammasome assays

Matured BMDMs were primed with LPS (500 ng/mL, Invivogen, #tlrl-3pelps) for 4 h in serum-free RPMI-1640 medium and then washed twice with RPMI-1640 medium. The cells were then treated with or without potassium chloride (Sigma-Aldrich, #1049360250) 30 min before stimulation with *C. perfringens* strain ATCC13124 (Guangdong Huankai Microbial Sci.&Tech.CO.,Ltd, #FSCC137003), CP1 or CP3 (clinical isolates of *C. perfringens*, specific 16S rDNA gene sequence data deposited at NCBI GenBank: MW440585 and MW440587) at a multiplicity of infection (MOI = 20) for 90 min, or one of the following stimulators: ATP (5 mM, 30 min, Sigma, #A2383), heat-killed bacteria (HK, MOI = 20, 90 min), bacterial culture supernatants (SN, 5 h), and bacterial α-toxin (20 μg/mL, 5 h), respectively. After treatment, the cell supernatants and lysates were collected for ELISA and western blotting assay. The LDH activities in the supernatants were determined by the LDH Cytotoxicity Assay kit® (Beyotime Biotechnology, #C0017) according to the manufacturer's protocols. Percent LDH release was calculated as (mean OD value of sample – mean OD value of blank)/(mean OD value of 1% TritonX-100 control sample – mean OD of blank) ×100. To analyze ASC speckles, the cells were stained with ASC primary antibody (Adipogen, #A29151803f) and Alexa Fluor® 488-conjugated anti-rabbit IgG secondary antibody (Abcam, #ab150077). The nuclei were stained with DAPI (2 μg/mL, Solarbio, #C0065). ASC speckles were visualized on a Laser Co-focus light microscopy (Nikon) and images were taken. To determine the bacterial killing capacity of BMDMs, LPS-primed BMDMs were incubated with rIL-18 (1000 pg/mL) or PBS for 1 h before infected with *C. perfringens* strain ATCC13124, CP1 or CP3 (MOI = 5) for 6 h, the supernatants were collected and plated on BHI agar plates to enumerate the bacteria after 24 h of anaerobic culture.

Extracellular traps formation assays

The matured BMDMs were seeded on 12-mm 0.01% poly-l-lysine–coated coverslips in 24 well-plates and then were incubated with LPS for 4 h before being infected with *C. perfringens* strain ATCC13124, CP1 or CP3 at a multiplicity of infection (MOI = 20) for 90 min, respectively. Cells were counterstained with Sytox Orange (5 μM, Invitrogen, #S-11368) and Hoechst 33342 (2 μM, Wanleibio, #WLA042a), and then were incubated with MPO primary antibody (Biorbyt, #orb16003), ELANE Polyclonal antibody (ABclonal, #A13015) or histone primary antibody (ABclonal, #A2348) and Alexa Fluor®488-conjugated anti-rabbit IgG secondary antibody (Abcam, #ab150077). Extracellular traps were visualized on a Laser Co-focus light microscopy (Nikon) and images were analyzed (Schindelin et al., 2012). To quantify extracellular traps formation,

extracellular DNA content in the supernatants were determined. LPS primed-BMDMs were stimulated with bacteria (MOI = 20), Sytox Green (5 μM, Invitrogen, #S7020) was added after 90 min. The cell supernatants were collected for fluorescence assay using a Varioskan Flash plate reader (Thermo Scientific).

Tissue histology and immunostaining

For histology, tissue samples of muscle, duodenum and cecum were fixed in 4% buffered formalin (Macklin, #P804536) solution and sections were stained with H&E to examine morphologic changes. For immunohistochemistry, tissue sections were stained with Ly-6G/Ly-6c (BioLegend, #108419), F4/80 (BioLegend, #123119), mucin 2 (Santa Cruz, #sc-515032), claudin 3 (Abcam, #A2946), and p-MLKL (Abcam, #ab196436) antibodies. For immunofluorescence, sections were stained with histone primary antibody (ABclonal, #A2348) and Alexa Fluor® 488-conjugated anti-rabbit IgG secondary antibody (Abcam, #ab150077). Meanwhile, apoptotic cell death in tissues were analyzed by TUNEL staining using a commercial kit (KeyGEN BioTECH, #KGA7061) following the manufacturer's instructions. DAPI (2 μg/mL) was used to stain nuclei. After sequential excitation, images were acquired utilizing a Laser Co-focus light microscopy (Nikon). For mucins secretion and glycosylation patterns assays, duodenal and cecal tissues were collected and stained with alcian blue as well as periodic acid–Schiff's reagent (AB-PAS staining, Solarbio, #1285) according to the manufacturer's manual.

Cytokine release analysis

Aseptically excised tissues were homogenized mechanically in cold PBS (at a ratio of 4 mL per gram tissue) containing 1% Triton X-100 (Sigma-Aldrich, #93443) and complete protease inhibitor cocktail (Sigma-Aldrich, #9036-19-5). Concentrations of various cytokines/chemokines in tissue homogenates or cell culture supernatants were measured by an ELISA assay following the R&D systems instruction.

Real-time PCR

Total RNA was extracted using TRI-reagent (Sigma-Aldrich, #T9424) according to the manufacturer's instruction. Subsequently, Quantitative real-time PCR assays were performed using SYBR Green (Roche, #04913914001) on an IQ5 Real-Time PCR Detection System (Bio-Rad). Gene expression levels were calculated using the $2^{-\Delta Ct}$ method. The following primer sequences were used: GAPDH sense 5′-CACCCCA GCAAGGACACTGAGCAAG-3′, antisense 5′-GG- GGGTCTGGGATGGAAATTGTGAG-3′. Occludin sense 5′-CAGCCTTCTGCTTCATCG-3′, antisense 5′-GTCGGGTTCACTCCCATTA-3′. ZO-1 sense 5′-GACCT TGAGCAGCCGTCATA-3′, antisense 5′-CCGTAGGCGATGGTCATAGTT-3′. Claudin 3 sense 5′-CCTAGG AACTGT- CCAAGCCG-3′, antisense 5′-CCCGTTTCATGGTTTGCCTG-3′.

Immunoblotting

Stimulated BMDMs or tissues were homogenized in lysis buffer solution [1% Triton X-100, 50 mM Tris-HCl (pH 7.4, Sigma-Aldrich, #10812846001), 150 mM NaCl (Sigma-Aldrich, #S3014), 0.1 mM Na3VO4 (Sigma-Aldrich, #S6508)] supplemented with a complete protease inhibitor cocktail, and supernatants of stimulated *BMDMs* were harvested and precipitated by methanol chloroform extraction to collect the cell lysate. The total lysates were separated by SDS-PAGE and transferred to PVDF membrane. The membranes were blotted with primary antibodies against Caspase-1 (Adipogen, #A28881708), IL-1β (Adipogen, #PRP1119-20μg), ASC (Adipogen, #A29151803f), GSDMD (Santa Cruz, #sc-393656), P38 MAPK (ABclonal, #A4771), p-P38 MAPK (ABclonal, #AP0526), JNK (Proteintech, #66210-1-Ig), p-JNK (ABclonal, #AP0276), ERK1/2 (ABclonal, #A10613), p-ERK1/2 (ABclonal, #AP0472), and GADPH (Roteintech, #60004-1-Ig).

QUANTIFICATION AND STATISTICAL ANALYSIS

Each experiment included 10 mice per group. Age-matched mice of both genders were included and randomly assigned to groups. Date are represented as mean ± SD. Differences between mean values of normally distributed data were assessed with one-way ANOVA (Dunnett's t-test) and two-tailed Student's t-test. Log-rank test was used for statistical analysis of animal mortality. *$p < 0.05$ and **$p < 0.01$ compared with control group. Statistical analysis was performed using Prism9 (GraphPad Software, La Jolla, CA, USA). The statistical values and details of the experiments can be found in the results, figure legends, and respective figures.